

Apparatus for Measurement of the Electric Dipole Moment of the Neutron using a Cohabiting Atomic-Mercury Magnetometer

C.A. Baker,¹ Y. Chibane,² M. Chouder,² P. Geltenbort,³ K. Green,¹ P.G. Harris,² B.R. Heckel,⁴ P. Iaydjiev*,¹ S.N. Ivanov†‡,¹ I. Kilvington,¹ S.K. Lamoreaux§,⁴ D.J. May,² J.M. Pendlebury,² J.D. Richardson,² D.B. Shiers,² K.F. Smith¶,² and M. van der Grinten¹

¹Rutherford Appleton Laboratory, Chilton, Didcot, Oxon OX11 0QX, UK

²University of Sussex, Falmer, Brighton BN1 9QH, UK

³Institut Laue-Langevin, BP 156, F-38042 Grenoble Cedex 9, France

⁴Department of Physics, University of Washington, Seattle, WA 98195

(Dated: September 29, 2018)

A description is presented of apparatus used to carry out an experimental search for an electric dipole moment of the neutron, at the Institut Laue-Langevin (ILL), Grenoble. The experiment incorporated a cohabiting atomic-mercury magnetometer in order to reduce spurious signals from magnetic field fluctuations. The result has been published in an earlier letter [1]; here, the methods and equipment used are discussed in detail.

PACS numbers: 13.40.Em, 07.55.Ge, 11.30.Er, 14.20.Dh

I. INTRODUCTION

A. The electric dipole moment of the neutron

Any non-degenerate system of defined, non-zero angular momentum will have a permanent electric dipole moment (EDM) d if its interactions are asymmetric under both parity (P) and time (T) inversion [2–4]. The neutron carries spin $\frac{1}{2}$, and it also possesses the virtue of being sensitive to all known particle physics interactions. It is therefore expected to possess a finite EDM with its magnitude dependent upon the nature and origin of the T violation, and this EDM is, in turn, a sensitive probe of such asymmetric interactions.

Parity violation [5] is a well-established property of the weak interaction in general. Evidence for T violation, which arises at a much weaker level, has come from the observation that there is a (0.66 ± 0.18) % greater probability for a \bar{K}^0 to turn into a K^0 than the other way around [6], and that there is an angular asymmetry in the rare decay $K_L \rightarrow \pi^+\pi^-e^+e^-$ of $(14.6 \pm 2.3 \pm 1.1)$ % [7, 8]. T violation and CP violation, where C is charge conjugation, are closely related through the CPT theorem [9–11] which predicts the invariance of the combined symmetry. Any CP violation in a CPT-invariant theory therefore implies the breakdown of time-reversal symmetry and leaves a finite expectation value of the neutron EDM. Violation of CP-symmetry has been studied

in detail in the K^0 system [12] and, more recently, in the B system [13, 14]; see, for example, [15] and references therein.

The origins of CP violation are still unknown. In the kaon system it is dominated by indirect ($\Delta S = 2$) contributions due to mixing. It has been observed [16, 17] in direct quark interactions ($\Delta S = 1$). Contributions from “superweak” $\Delta S = 2$ interactions specific to the kaon systems have been ruled out.

Many alternative theories exist (see, for example, contributions in [18]), but the data from the K^0 and b systems alone are insufficient to distinguish between them. These theories also predict non-zero values for the EDM of the neutron, but the predictions differ, one from another, by many orders of magnitude [19]. The major difference between the theories is that in some, and in particular in the standard $SU(2) \times U(1)$ model of electroweak interactions, the contributions to the EDM appear only in second order in the weak interaction coupling coefficient, whereas in others the contributions are of first order in the weak interaction. Detection of the latter larger size of EDM would be evidence for new physics beyond the standard model [20]. The small size of the neutron EDM, as indicated by the measured values displayed in Fig. 1 [1, 21–37], has already eliminated many theories, and is pressing heavily upon the expectations from extensions to the Standard Model through to supersymmetric interactions.

B. Implications of non-zero EDM measurements

EDMs are being sought in various systems: the free neutron, the mercury atom [38], and the electron (via the thallium atom [39] and, more recently, the YbF [40] and PbO molecules [41]), in addition to a proposal to study deuterium [42]. The fundamental mechanisms underlying sources of EDMs are different in each system, and the

*On leave of absence from INRNE, Sofia, Bulgaria

†On leave of absence from Petersburg Nuclear Physics Institute, Russia

‡Present address: Institut Laue-Langevin, BP 156, F-38042 Grenoble Cedex 9, France

§Present address: Department of Physics, Yale University, New Haven, CT 06520

¶deceased

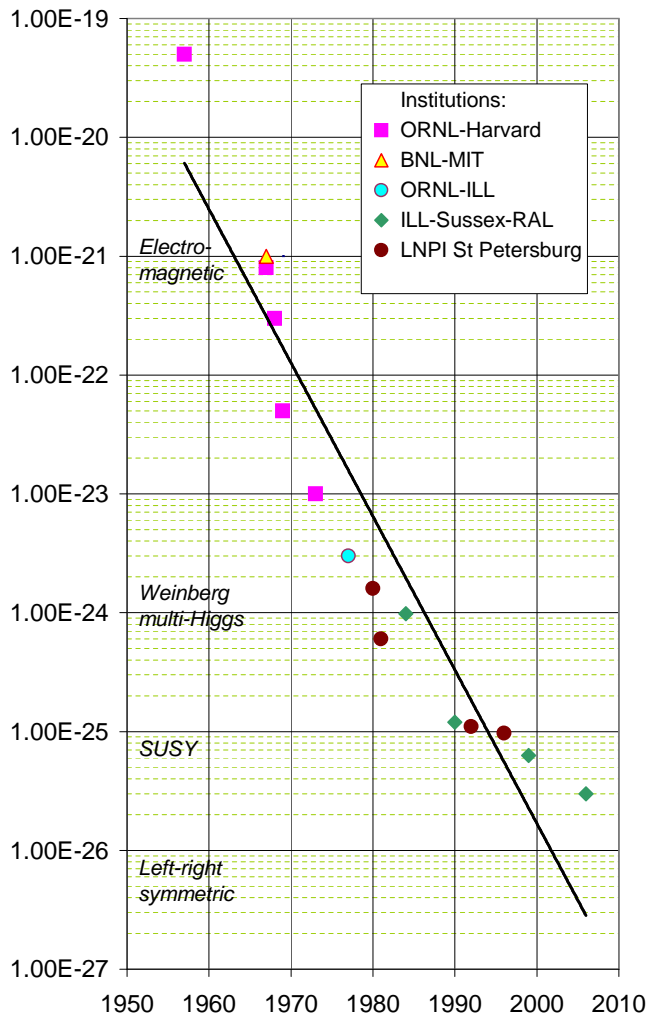


FIG. 1: (Color online) The evolution of the experimental limit of the electric dipole moment of the neutron. Those experiments before 1980 used neutron beams, and those after used stored ultracold neutrons. See [19] for the theoretical predictions.

measurement of a finite value within one of these systems would therefore have distinctive implications [43]: For example, if the EDMs are driven by the QCD θ angle, one would expect similar contributions to all strongly coupled systems, with the consequent approximate pattern $d_n \sim d_{Hg} \sim d_D \gg d_e$, and so on. Thus, the different systems have different implications for physics models beyond the standard model. Measurements on multiple systems are also needed in order to rule out cancellations.

EDM limits provide fairly tight constraints upon supersymmetric models; the same is true of most other models beyond the standard model that attempt to incorporate CP violation to a degree adequate to explain the observed baryon asymmetry of the Universe. The “accidental” cancellation of first-order contributions in the Standard Model is not a general feature, and EDM

limits (and EDM values, once measured) provide a powerful way to distinguish between models and, indeed, to eliminate many of them. Ramsey [44] and Barr [17] have provided useful reviews of the situation, and the book by Khriplovich and Lamoreaux [45] contains further general information on EDMs.

II. PRINCIPLE OF THE METHOD

Almost all of the experimental searches for the EDM of the neutron have been magnetic resonance experiments in which polarized neutrons are subjected to parallel magnetic and electric fields in vacuum [46],[47]. The only internal degrees of freedom of the neutron are those associated with the spin \mathbf{s} , so that the Hamiltonian (\mathcal{H}) in an electric (\mathbf{E}_0) and a magnetic (\mathbf{B}_0) field is

$$\mathcal{H} = -2\mathbf{s} \cdot (\mu_n \mathbf{B}_0 + d_n \mathbf{E}_0). \quad (1)$$

If the magnetic and electric fields are parallel or antiparallel, the precession frequency ν_0 of the spin is given by

$$h\nu_0 = -2\mu_n |\mathbf{B}_0| \mp 2d_n |\mathbf{E}_0|, \quad (2)$$

where h is Planck’s constant, μ_n is the magnetic dipole moment ($-1.913 \dots$ nuclear magnetons), d_n is the EDM and the upper (lower) sign is for \mathbf{B}_0 and \mathbf{E} parallel (antiparallel). When an electric field of magnitude E_0 is changed from being parallel to \mathbf{B}_0 to being antiparallel, the precession frequency changes by

$$\delta\nu_0 = -\frac{4d_n E_0}{h}. \quad (3)$$

An EDM of 10^{-25} e cm would give a frequency shift of 1μ Hz with the reversal of a 1 MV/m electric field. Because μ_n is negative, the sign definition for d_n is such that a positive dipole moment would increase the precession frequency when \mathbf{E} and \mathbf{B}_0 are antiparallel. Application of a magnetic field produces a magnetic Zeeman splitting; subsequent application of an electric field then merely changes the separation of the Zeeman levels, without inducing any further splitting. It should be noted that the electric polarizability of the neutron cannot affect the precession frequency to first order.

The early experiments used beams of neutrons with velocities greater than 100 m/s. Such experiments became limited by the $\mathbf{v} \times \mathbf{E}$ effect, according to which motion through the electric field results in a magnetic field in the neutron rest frame and hence a possible change in the precession frequency with the same dependence on the electric field as a real EDM. More recent experiments use ultra-cold neutrons (UCN), with velocities of less than 7 m/s, stored in evacuated chambers with walls that totally reflect the neutrons; the average velocity is so close to zero that the $\mathbf{v} \times \mathbf{E}$ effect can be adequately controlled at the present level of sensitivity. The first published result from a series of experiments being carried out under these conditions at the Institut Laue-Langevin (ILL) in

Grenoble was $d_n = -(3 \pm 5) \times 10^{-26}$ e cm [34]. A broadly similar experiment at the PNPI in Russia [36] yielded an EDM of $(+2.6 \pm 4.0 \pm 1.6) \times 10^{-26}$ e cm. Both experiments were limited at the time by systematic uncertainties associated with instabilities and non-uniformities in the magnetic field. The ILL experiment initially used three rubidium magnetometers adjacent to the storage cell to try to compensate for magnetic field drifts; the PNPI experiment used instead a back-to-back twin-cell arrangement to make simultaneous measurements with the \mathbf{E} field in opposite directions. In each case, the presence of gradients in the magnetic field could adversely affect the results, since there was a significant displacement between each measurement cell and the control volume used for compensation. This problem was addressed in this experiment at the ILL by the installation of a magnetometer based upon measurement of the precession frequency of spin-polarized $I = 1/2$ atoms of ^{199}Hg (3×10^{10} atoms/cm³; $\mu_n/\mu_{Hg} = \gamma_n/\gamma_{Hg} = -3.842$) stored simultaneously in the same trap as the neutrons. Using Eq. (2) for both the neutrons and the mercury, and assuming that both experience the same B , we find that to first order in the EDMs d ,

$$\frac{\nu_n}{\nu_{Hg}} = \left| \frac{\gamma_n}{\gamma_{Hg}} \right| + \frac{(d_n + |\gamma_n/\gamma_{Hg}| d_{Hg})}{\nu_{Hg}} E = \left| \frac{\gamma_n}{\gamma_{Hg}} \right| + \frac{d_{meas}}{\nu_{Hg}} E. \quad (4)$$

It is worth noting that Eq. (4) is only valid in a non-rotating reference frame. The rotation of the Earth imparts a small but perceptible shift in this frequency ratio [48].

For each data-taking run, the measured EDM d_{meas} was obtained from a linear fit to the ratio ν_n/ν_{Hg} versus E . Eq. (4) shows that d_{meas} contains a contribution from d_{Hg} . The true d_{Hg} has been shown to be $(-1.06 \pm 0.49 \pm 0.40) \times 10^{-28}$ e cm [38], so it introduces a systematic error of $(-0.4 \pm 0.3) \times 10^{-27}$ e cm into d_{meas} .

To the true d_n and d_{Hg} within d_{meas} there will also be added coefficients of fractional shifts in ν_n and ν_{Hg} , from other causes, which are linear in E and thus constitute additional systematic errors. The most important of these involves a geometric phase (GP) arising when the trapped particles experience a gradient $\partial B_{0z}/\partial z$ in the presence of E [49]. This particular effect has now been characterised and understood, and to a large extent it has been possible to compensate for it.

III. ULTRACOLD NEUTRONS

As a consequence of the coherent strong interaction between neutrons and the nuclei of a material medium, the surface of the medium presents a potential step relative to vacuum for long-wavelength neutrons. This potential V_F , called the mean Fermi potential, is given by [50]

$$V_F = \frac{2\pi\hbar^2}{m} N b, \quad (5)$$

where m is the mass of the neutron and N the number of atoms per unit volume with mean coherent forward scattering length b . A neutron with velocity less than the critical velocity v_c , defined by $mv_c^2/2 = V_F$, will be reflected from the surface for any angle of incidence. The Fermi potential for most materials is less than 300 neV, which corresponds to critical velocities of less than 7.6 m/s. Such slow neutrons can be confined in material traps by total external reflection, and are called ultra-cold neutrons (UCN). Nuclear reactors are a source of UCN, which constitute the very low energy part of the spectrum of moderated neutrons.

For cold and ultra-cold neutrons in a magnetic material the Fermi potential due to the nuclear scattering acquires an additional term representing the interaction of the magnetic moment of the neutron μ_n with the internal magnetic field B of the material. Thus,

$$V_F = \frac{2\pi\hbar^2}{m} N b \pm \mu_n B, \quad (6)$$

where the \pm refers to the two spin states of the neutron. It is possible to find ferromagnetic materials with very low Fermi potentials for one spin state of the neutron and high Fermi potentials for the other spin state. It is then possible to spin-polarize UCN by transmission through a thin magnetised foil of such a material.

In the experiment described in this paper the number density of UCN was less than 10 cm^{-3} , and hence neutron-neutron collisions were extremely unlikely and can be ignored.

A. Upscattering and absorption of UCN in materials

Although the UCN have speeds characteristic of a temperature of about 2 mK, the neutron storage trap was maintained at room temperature. At first sight it might appear surprising that these neutrons could be stored for hundreds of seconds without being scattered out of the UCN energy range. This was possible because the thermal motions of individual nuclei in the walls of the trap were sensed only weakly by the UCN, which were reflected by the combined coherent scattering from millions of nuclei lying within a short distance (of the order of 100 Å) of the surface. In this coherent scattering, the thermal motion of the center of mass of such a large group was negligible compared with the speed of the UCN. At the same time, any recoil energy associated with the group was also negligible. In addition, collisions that involved an exchange of energy with a smaller group of nuclei in the wall, and hence an upscattering of the neutron out of the UCN energy range, were infrequent (although important in determining the mean storage lifetime): the following argument has been given by Zeldovich [51]. When a neutron is reflected from a surface, its wave function penetrates into the wall a distance of order $(\lambda/2\pi)$, where λ is the de Broglie wavelength. In a storage volume of

dimension l , each neutron with velocity v which is stored for a time T_s accumulates a total path length L inside the material of the walls, where

$$L \approx \frac{\lambda T_s v}{2\pi l}. \quad (7)$$

For the typical values of $T_s = 150$ s, speeds v of up to about 5 m/s, and $l = 150$ mm, a value of $L = 60 \mu\text{m}$ is obtained. This distance is sufficiently small, compared with observed UCN interaction lengths, that one expects very little inelastic scattering and absorption of the neutrons.

In general, the survival times of UCN in material traps, particularly those made from materials with low absorption cross sections, are less than would be calculated for pure materials. This is caused by the presence of impurities (particularly hydrogen) in the surface, which drastically reduces the survival time [52, 53]. To reduce hydrocarbon contamination of the trap used in this EDM experiment, the majority of pumps in the vacuum system were oil-free turbopumps; the remaining diffusion pumps were filled with Fomblin [54] oil, which is a fully fluorinated polyether [55]. The chemical formula of Fomblin is $\text{CF}_3(\text{OCF}_2\text{CFCF}_2)_m(\text{OCF}_2)_n\text{OCF}_3$. To reduce the presence of surface hydrogen still further, the trap surfaces were discharge-cleaned using 1 torr of oxygen.

B. Depolarization in wall collisions

If neutrons are stored in a trap made of a material with non-zero magnetic moments, the interaction between a neutron and the wall will be spin dependent. Collisions with the walls will therefore result in depolarization of the neutrons. The magnitude of this depolarization can be estimated using a simple random walk model, similar to that of Goldenberg, Kleppner and Ramsey [56]. If, during one collision with the wall, the two spin states of the neutron experience Fermi potentials that differ by ΔV_F , and the interaction lasts a time τ , the spin of a neutron will be rotated through an angle

$$\delta\phi \approx \frac{\tau \Delta V_F}{\hbar}. \quad (8)$$

For the case where the neutron penetrates a distance $\lambda/2\pi$ into the wall,

$$\tau = \frac{\lambda}{2\pi v} \approx 2 \times 10^{-9} \text{ s}. \quad (9)$$

During the storage time the neutron makes $M = T_s v/l$ collisions with the walls, for which the phase shifts, which differ randomly from one wall collision to another, will add as in a random walk, so that the overall rms phase shift is

$$\Delta\phi \approx \overline{\delta\phi} \sqrt{M} = \frac{\overline{\Delta V_F} \lambda}{\hbar} \sqrt{\frac{T_s}{lv}}. \quad (10)$$

If the difference in Fermi potentials is ΔV_F for a material in which all of the nuclei are aligned, a neutron that interacts with N randomly oriented nuclei will experience an average potential difference of $\overline{\Delta V_F} = \Delta V_F / \sqrt{N}$. The number of interacting nuclei is $N \approx n (\lambda/2\pi)^3$, and, taking $\Delta V_F = V_F = 250$ neV, $n = 10^{29} \text{ m}^{-3}$, $T_s = 130$ s, $v = 6 \text{ m s}^{-1}$ and $l = 150$ mm, a phase difference of

$$\Delta\phi \approx 0.02 \text{ rad} \quad (11)$$

is obtained. This implies that polarized neutrons can retain their polarization for times of the order of 10^5 s. In practice, the depolarization time in the storage trap used for this EDM experiment was of the order of 600 s.

It follows from the above that the ability to store polarized neutrons is exclusive to storage traps that are made of non-magnetic materials. If the walls of the trap contain magnetic domains of size comparable to or greater than the neutron wavelength, then the interaction of the magnetic moment of the neutrons with the magnetic field inside the domains dominates. Since the magnetic interaction can be a few hundred neV, the same size as V_F , one effectively suppresses the factor of $1/\sqrt{N}$ in the above calculation and the neutron polarization survival time drops to values of the order of 50 ms.

IV. RAMSEY'S METHOD OF SEPARATED OSCILLATING FIELDS

The precession frequency of the stored neutrons was determined by the method of separated oscillating fields. The method was devised for molecular beam experiments where an oscillating field is applied to the beam at the beginning and at the end of a flight path through an interaction region [57, 58]. In this EDM experiment, where the neutrons were stored in a trap, two short intervals of phase-coherent oscillating field were applied, one at the beginning and the other at the end of a period of free precession, so that they were separated in time but not in space. The phase coherence between the two pulses is achieved by gating off the output of a single oscillator during the intervening period. The sequence is shown schematically in Fig. 2.

At the start of each measurement cycle within a data-taking run, the neutrons passed through the magnetised polarizing foil and entered the storage volume with their spin polarization antiparallel to the uniform magnetic field \vec{B}_0 (a state referred to henceforth as ‘‘spin up’’). A resonant oscillating field \mathbf{B}_1 , perpendicular to \mathbf{B}_0 and with a frequency close to resonance, was applied for 2 seconds with an amplitude such that the neutron polarization vector was rotated through an angle of $\pi/2$ and brought perpendicular to \mathbf{B}_0 . The polarization vector was then left to precess about \mathbf{B}_0 during a period T_{fp} (the subscript here indicating ‘‘free precession’’), until the second phase-coherent oscillating field pulse was applied. If the oscillating field frequency had been exactly on the center of the resonance, this second pulse would

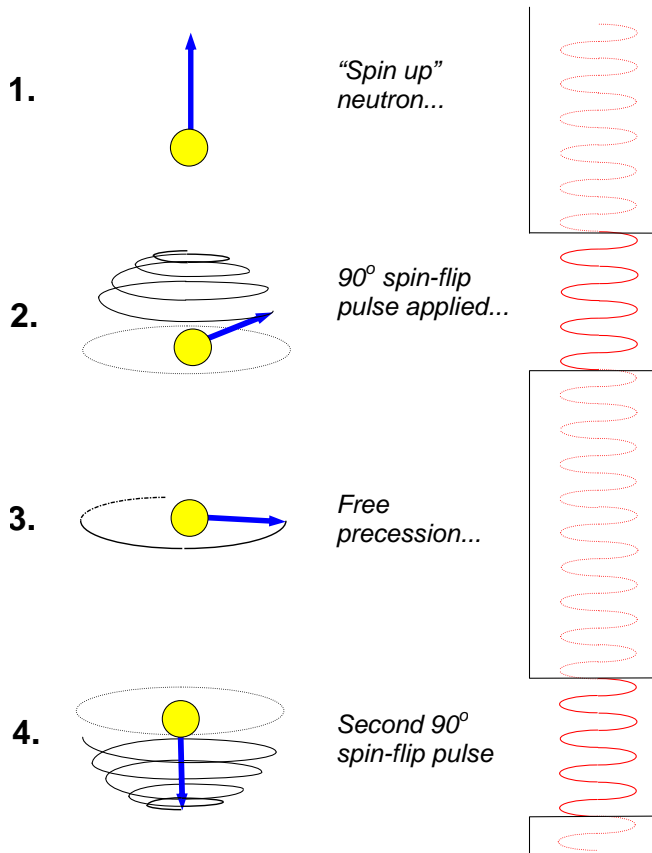


FIG. 2: (Color online) The Ramsey method of separated oscillatory fields. See text for description.

have rotated the polarization through a further $\pi/2$ such that it became parallel to \mathbf{B}_0 (the \hat{z} direction), as shown in Fig. 2. For frequencies a little off resonance, the final \hat{z} -component of the polarization depends strongly on the accumulated phase difference between the neutron polarization vector and the oscillator. When the neutrons were finally released from storage, the magnetised polarizing foil served as an analyzer, giving a neutron count that depended linearly upon this final \hat{z} component of the polarization. Thus, the neutron count was sensitive to the accumulated precession phase.

Emptying the trap and counting the stored neutrons took 40-50 s. For half of this time, a 20 kHz oscillating current was applied to a solenoid wrapped around the guide tube above the polarizer. This flipped the spins of the neutrons, and allowed the neutrons in the opposite spin state (“spin down”) to be counted.

Fig. 3 shows the Ramsey resonance pattern obtained experimentally as the frequency of the oscillating field \mathbf{B}_1 was varied. It is expected theoretically [57, 58] that, across the central fringes, the number of neutrons counted as a function of the oscillating field frequency ν

can be described by

$$N_{\uparrow\downarrow}(\nu) = \bar{N}_{\uparrow\downarrow} \mp \alpha_{\uparrow\downarrow} \bar{N}_{\uparrow\downarrow} \cos\left(\frac{\pi(\nu - \nu_0)}{\Delta\nu}\right), \quad (12)$$

where \bar{N} is the average number of neutrons counted for the spin state in question, up \uparrow or down \downarrow . The visibility α is the product of the neutron polarization and analyzing power, again for the spin state in question; ν_0 is the resonant frequency, and the linewidth $\Delta\nu$ is the width at half height of the central fringe. The two signs \mp also refer to the two spin states. \bar{N} and α (for either spin state) are related to the fringe maximum and minimum N_{\max} , N_{\min} as follows:

$$\bar{N} = \frac{(N_{\max} + N_{\min})}{2},$$

$$\alpha = \frac{(N_{\max} - N_{\min})}{(N_{\max} + N_{\min})}.$$

Given a time T_{fp} between the two oscillating field pulses, if the oscillating field is applied for a time t at both the beginning and the end of the storage time then the linewidth $\Delta\nu$ is given by [59]

$$\Delta\nu = \frac{1}{2(T_{fp} + 4t/\pi)} \quad (13)$$

$$\approx \frac{1}{2T_{fp}}, \text{ if } 4t/\pi \ll T_{fp}. \quad (14)$$

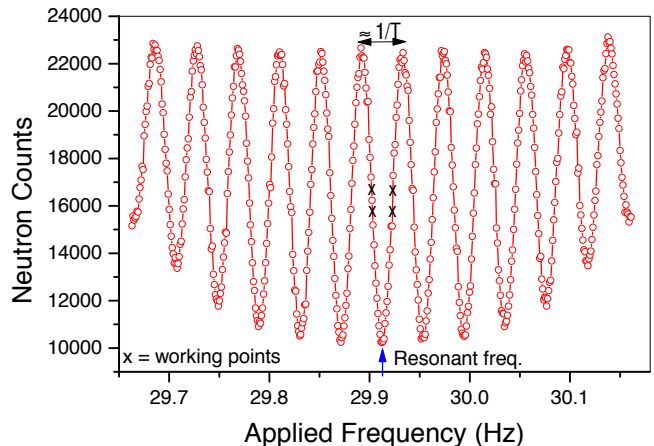


FIG. 3: (Color online) The Ramsey resonance pattern obtained by scanning the frequency of the oscillating field \mathbf{B}_1 through the resonance. The coherence time (between the Ramsey pulses) was 22 s in a 1 μ T magnetic field. The ordinate is the number of neutrons in the original spin state counted at the end of each storage time. Error bars are omitted for clarity. During normal data taking measurements were taken sequentially at the four points shown.

Eq. (12) may be differentiated to obtain

$$\frac{dN}{d\nu} = \frac{\pi}{\Delta\nu} \alpha \bar{N} \sin\left(\frac{\pi(\nu - \nu_0)}{\Delta\nu}\right). \quad (15)$$

The measurements were made at $\nu \approx \nu_0 \pm \Delta\nu/2$, where the number of neutrons counted was $N_{\uparrow\downarrow} \approx \bar{N}_{\uparrow\downarrow}$ for each spin state, giving a total of $N \approx \bar{N}_{\uparrow} + \bar{N}_{\downarrow}$ neutrons per measurement cycle. The fractional uncertainty in the number of neutrons counted is at best $1/\sqrt{N}$, so the uncertainty in the measurement of the frequency is no better than

$$\begin{aligned} \sigma_\nu &= \frac{\Delta\nu}{\pi\alpha\sqrt{N}} \\ &\approx \frac{1}{2\pi\alpha T_{fp}\sqrt{N}}. \end{aligned} \quad (16)$$

In the case of a perfectly constant magnetic field, the EDM could be calculated from the difference in precession frequency between the two directions of the electric field. For a total (over a number of measurement cycles) of N_T neutrons, equally divided between the two directions of the electric field, the uncertainty in the EDM due to neutron counting statistics would be

$$\sigma_d \approx \frac{\hbar}{2\alpha E_0 T_{fp} \sqrt{N_T}}. \quad (17)$$

This result, which is applicable when the noise does not exceed that due to normal counting statistics, corresponds to the fundamental limit of sensitivity given by Heisenberg's uncertainty principle: the uncertainty in frequency is inversely proportional to the observation time T_{fp} .

It is desirable for the systematic error in absolute frequency to be as low as 0.2 ppm. In the neutron case there is a significant upward shift created by the Ramsey-Bloch-Siegert (RBS) effect [60, 61]. In the EDM data taking cycle, this shift is calculated to be 0.15 ppm. Other systematic-error frequency shifts, such as that due to the rotation of the Earth, are discussed in [1] and [62].

One of the great virtues of the Ramsey method is the symmetry of the central fringe about the true Larmor frequency (plus RBS shift), even when the fringes are smeared by field inhomogeneities. In this experiment the Ramsey pattern contained about 100 fringes, and the field was homogeneous to 0.1%.

Under normal running conditions, the magnetic field drifted slowly. However, the frequency measurements of the mercury magnetometer allowed us to set up a neutron resonance frequency on the synthesizer unfailingly extremely close to the desired part of the central fringe, and thereby to compensate for the magnetically induced frequency shifts within each measurement cycle. The precision of the Hg magnetometer was sufficient for the uncertainty on d_n to be dominated by neutron counting statistics, such that equation (17) still applies. Fig. 4 shows a typical set of data from a single run, fitted to the Ramsey curve. The spread of points along the curve arises from the shifts in the magnetic field from one batch cycle to another.

The data points of Fig. 5 show, on a log scale, the distribution (over the entire data set) of stretch values r_i

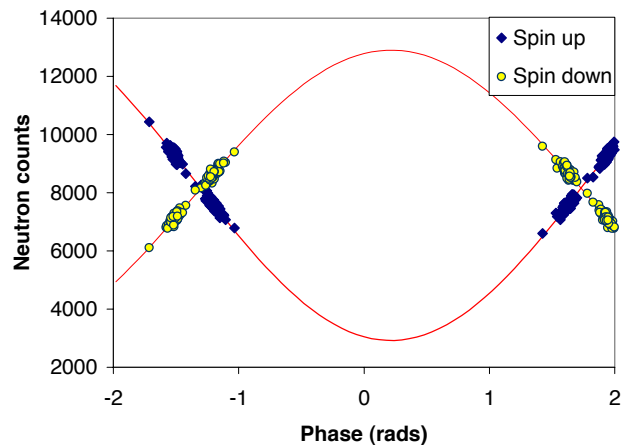


FIG. 4: (Color online) Spin-up and spin-down neutron counts for a single run fitted to the Ramsey curve (Eq. 12).

of the fits to the Ramsey curve:

$$r_i = \frac{(\nu_i - \nu_{R_i})}{\sigma_i}, \quad (18)$$

where ν_i is the calculated frequency of the i th batch of neutrons, σ_i is its uncertainty and ν_{R_i} is the expected frequency for that batch as determined by the mercury magnetometer, the applied r.f. and the Ramsey curve function. Ideally, and in the absence of any EDM-like signals, this distribution would be expected to be a Gaussian of unit width. The continuous line is a Gaussian of width 1.06. The true distribution departs from this Gaussian at about 4σ . The few points lying outside this range tend to be associated with runs that have other known problems, for example with intermittent failure of the neutron delivery system. Because of the symmetric way in which the data were taken, rejecting batches that lie within the tails from this distribution cannot of itself induce a false EDM signal.

V. EXPERIMENTAL APPARATUS

A schematic of the experimental apparatus is shown in Fig. 6.

A. The neutron subsystem

1. Neutron production and transport

Very cold neutrons with a speed of about 50 m/s are extracted from the liquid-deuterium cold source of the 58 MW high-flux ILL reactor, through a vertical guide known as the TGV (*tube guide verticale*). These neutrons are incident on the Steyerl turbine[63, 64] which converts them to UCN by reflection from the (receding)

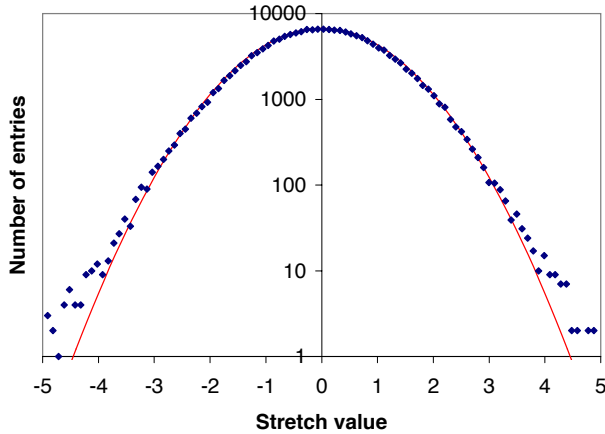


FIG. 5: (Color online) Distribution of stretch values from the fits to the Ramsey curve

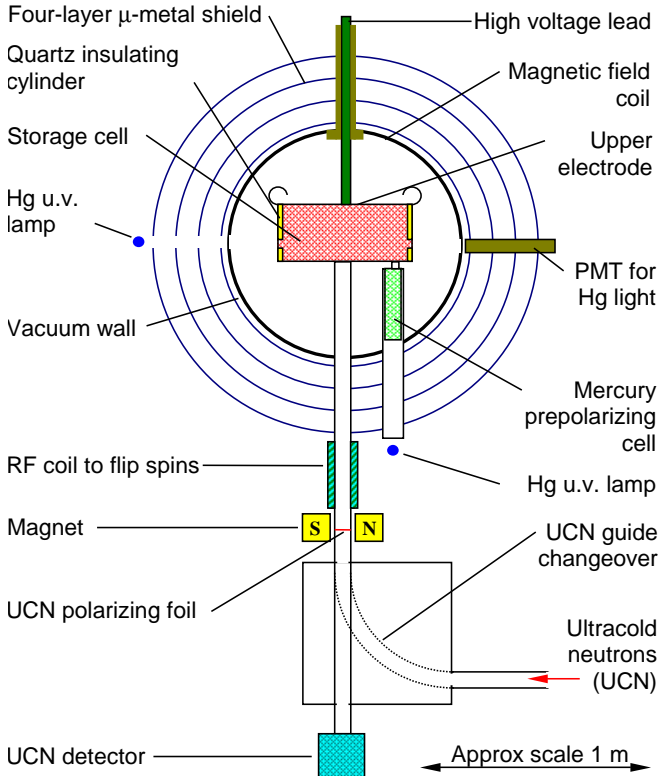


FIG. 6: (Color online) The neutron EDM experimental apparatus

turbine blades. The UCN exiting from the turbine can be directed to several experimental positions by computer-controlled switching of horizontal UCN guides. At the entrance to the horizontal guide of the EDM position, the turbine blades produce a phase space density (PSD) of $0.084 \text{ UCN (m/s)}^{-3} \text{cm}^{-3}$, which remains constant up

to a UCN velocity of 8 m/s, or an energy equivalent to 3.2 m fall in height. This PSD can provide 87 UCN/cm^3 in a natural nickel bottle, 71 UCN/cm^3 in a stainless steel bottle and 25 UCN/cm^3 in a vitreous quartz bottle of height 0.12 m. The latter density is the most relevant since the sidewall of the EDM measurement bottle was made of vitreous quartz and was 0.12 m high. These numbers are ‘real UCN’[64] in that they do not allow for the reduction on conversion to counts caused by the efficiency 0.80 ± 0.05 of the UCN detector.

The UCN guide from the turbine blades to the EDM bottle had a total length of 9.2 m divided into a horizontal length of 7.1 m followed by a vertical length to the upper surface of the lower electrode of 2.08 ± 0.05 m. This latter figure is the height above the UCN source of the DLC surface of the bottle lower electrode. Thus, UCN need to have an energy corresponding to 2.08 m of height at the source in order to only just reach the lower electrode surface, and to have an energy corresponding to 3.00 m of height at the source in order to enter the EDM bottle with the highest fully containable energy of 0.92 m at the lower electrode surface. This range of energies at the source is within the range of its uniform brightness. Thus a perfect 9.2 m of guide with no polarizer and no safety window in place, and no annihilation of UCN, would fill the EDM bottle to 25 UCN/cm^3 .

We have used diffusion theory[50] to model the filling of the bottle with the real guides and their losses. The guides had three types of surface: natural nickel evaporated onto thin glass for 1.8 m in the turbine house, with cross section 70 mm x 70 mm; $^{58}\text{NiMo}$ sputtered onto electro-polished stainless steel surfaces for 5.9 m from the turbine house to the position of the polarizer, with circular cross section of diameter 78 mm; and Be sputtered onto glass for the 1.5 m above the polarizer to the EDM bottle, again circular in cross section, with a diameter of 65 mm. The theory indicates that at the completion of a long filling of the EDM bottle, the guide system, including the 0.1 mm thick aluminium safety window, is attenuating the PSD at the base of the bottle relative to that of the UCN source by a factor of 0.55 for the lowest energy UCN that can enter the bottle and by a factor of 0.22 for the highest energy UCN that can be contained in the bottle. This represents a considerable softening in the UCN spectrum in the bottle compared to a Maxwell spectrum with the quartz cut-off. There are three mechanisms involved in this softening. First, the UCN that can only just enter the bottle are on the point of marginally exceeding the lower (2.0 m) Fermi potential energy in the (ferro-magnetic) nickel surface of the guide in the turbine house. This energy excess increases to 1.0 m height equivalent at the top end of the bottle spectrum, and causes much leakage of these UCN through the nickel guide wall. The result is a 30% relative reduction in the UCN PSD at the top end relative to the bottom end of the bottle spectrum. Secondly, the performance of the entire guide system deteriorates with increasing UCN energy since both the UCN losses in guide wall re-

flections and their diffuse reflection probabilities increase with UCN energy. This results in a further 29% relative reduction in PSD at the top end. Lastly, the UCN current drawn from the guide by the UCN losses in the EDM bottle itself also increases with UCN energy, causing a relative reduction of 17.5%. When the polarizer is inserted, these last attenuations are slightly more than those just given.

The diffusion model just referred to has just one adjustable parameter, which represents the probability of diffuse reflection per collision for UCN with a total energy equal to the critical energy. All of the guide surfaces have thin sputtered or evaporated coatings on highly polished substrates. The parameter was adjusted to give the observed number of UCN just after filling for our EDM bottle after five filling time constants. Agreement with experiment on UCN densities was therefore ensured. The probability of diffuse reflection per collision deduced from the fit for UCN at the local critical energy was found to be 0.075. In independent experiments, we have found a corresponding value of 0.040 for uncoated lightly electropolished honed stainless steel surfaces. [65, 66] This suggests that coating processes increase the surface roughness for the surface wavelengths that are short enough to produce totally diffuse reflections. For UCN with an isotropic distribution of velocities and kinetic energy equal to half of the critical energy our probability of diffuse reflection per collision on the coated surfaces would be $0.075/2 = 0.038$. In the case of uncoated stainless steel this last figure would be 0.02.

The main value of the diffusion calculation has been the determination of the shape of the UCN energy spectrum used for the EDM measurement. The spectrum shape is important in understanding some of the later results. Although the softening of the spectrum reduces UCN numbers, it increases the average UCN storage time more than in proportion to the reduction of UCN energy. This largely cancels the reduction in sensitivity of the EDM measurement by allowing the use of a longer Ramsey resonance time. The softening also increases the average height difference due to gravity between the stored UCN and the stored Hg atoms. Knowledge of the UCN spectrum allows one to calculate this height difference, which is needed for a method of assessing the systematic errors caused by geometric phases.[49] This height difference can also be determined using magnetic resonance, with a containment trap of variable height. This gives results in good agreement with that calculated from the UCN spectrum. This UCN spectrum is also successful in fitting the observed UCN counts versus storage interval for all intervals between 60 s and 600 s to within the RMS noise of about 2% arising from fluctuations in shutter timing. At zero containment time there appears to be a 25% UCN excess due to the presence of UCN that are not fully contained. At a containment time of 60 s these extra UCN appear to have fallen below the 2% noise level.

The spectrum-weighted average attenuation of the

PSD in the EDM bottle filling process was a factor of 0.295 relative to the UCN source. This led to an initial density of fully contained UCN in the bottle, after a long filling time with no polarizer and on just closing the door, of 7.5 fully contained UCN/cm³ and a total number of 160,000 UCN. The latter number falls to 69,400 after the containment interval of 140 s used when taking EDM data. To find the final UCN counts from an EDM data-taking cycle we must take account of further attenuations to the figure of 69,400 per batch. These are (i) 0.727 for curtailment of the filling and emptying intervals to conserve polarisation and batch cycle duration (ii) 0.525 for spin selection, which includes a small increase due to production of wrong spins (iii) 0.80 for the combined loss in two transits of the polarizer foil (iv) 0.875 for losses when waiting for the spin flipper while the other spin state is counted (v) 0.915 for guide losses in transit from the bottle to the detector (vi) 0.80 for detector efficiency. These figures indicate a final count of 13,600 per batch - close to the 14,300 observed average count from all runs.

We believe that the spectrum changes derived from these last attenuations are small and partly cancelling - process (i) gives a slight hardening (ii) and (iii) and (vi) are neutral while (iv) and (v) induce a slight softening.

In order to deal with the variety of surfaces involved, a simple model has been adopted for estimating the parameter η to be used with the theoretical energy dependence in calculating the UCN loss probability per collision. Our model takes $\eta = (\eta_A + \eta_H)$, where η_A is the contribution for the atomic composition of the material excluding hydrogen and η_H is the contribution from interstitial hydrogen. We are concerned with the situation where none of the materials has been baked in vacuum. From measurements on 316-type stainless steel[67] we take $\eta_H(\text{SS})$ to be 3.9×10^{-4} and for other materials X we take $\eta_H(\text{X}) = \eta_H(\text{SS}) \times (V_{\text{SS}}/V_{\text{X}})$, where the V s are the mean Fermi potentials. This amounts to assuming that, at room temperature, the atomic fraction of hydrogen and the UCN loss cross-section for hydrogen are the same in the surface layers of all the materials concerned. In our experience this model works well in predicting lifetimes to about 20% in wide variety of bottles and guide tubes made of unbaked materials at room temperature.

The key data used in this assessment arose from a data-taking run labelled ALP1120.dat, which produced data for UCN counts versus containment time in steps of 5 s up to 660 s. It used a large smooth-sided bottle with a period of 60 s used for filling and 70 s for emptying, with no polarizer present. Only the emptying process enters to cause the data count totals to differ from the actual number of real UCN in the bottle when the shutter is opened for emptying. This difference involves just two factors: (i) the detector efficiency, and (ii) UCN lost in the emptying guide and in the bottle after the shutter is opened. The detector efficiency is generally assessed as 0.80 ± 0.05 , with losses in the window and loss of counts below the discrimination level each being about 0.10. The over-

all emptying time constant after 140 s of containment was measured in a separate run, labelled ALP1115.dat, to be 9.35 ± 0.30 s. After this containment, the bottle UCN lifetime is about 210 s, so the fractional bottle loss during emptying is to first order $9.4/210 = 0.045$. To calculate losses in the guide we need the average time spent in the guide by each UCN before it is detected, and the storage time of the guide. The latter is typically 20 s. If the guide were to be perfectly smooth the time to the detector would be the free-fall time, which is 0.4 s; however, the guide has some roughness, and we can estimate from the emptying time constant that about 40 % of the UCN that leave actually return to the bottle. Assuming that the roughness approximately doubles the time taken, making 0.8 secs, the fractional loss would be $0.8/20 = 0.04$, making a total emptying loss of $0.045 + 0.04 = 0.085$. We are now in a position to calculate the real number of stored UCN. Then, knowing the turbine performance [63, 64], we have the overall loss in the entry guide system, which allows us to fix the roughness parameter.

2. The neutron polarizer

The neutrons were polarized by transmission through a silicon foil upon which was deposited a $1 \mu\text{m}$ layer of iron that was magnetised close to saturation by a field of about 0.1 T from a permanent magnet. This had Fermi potentials of approximately 90 and 300 neV for the two spin states of the neutron. The foil was mounted 1.5 m below the trap, so that neutrons that had sufficient energy to penetrate the foil could slow down before reaching the trap.

The polarizer was mounted with the magnetized layer towards the trap, since experience in the past showed that this orientation gave the better neutron polarization. With neutrons that made a single passage through the foil, such polarizers can produce a transmitted neutron polarization in excess of 90% [68]. However, they do have a finite probability, of a few percent, of flipping the spin of both transmitted and reflected neutrons. In this case it led to a build-up of neutrons in the unwanted spin state as the trap filled, thus reducing the polarization that was finally achieved. The maximum polarization was obtained for very short filling times [69]. The filling time was therefore adjusted so as to maximize $\alpha\sqrt{N}$.

As mentioned above, the 1.5 m of neutron guide between the polarizer and the neutron trap was made of glass, with the inner surface coated with BeO, which is non-magnetic. This guide was used instead of a stainless steel guide because remnant magnetization and magnetic domain structure in a stainless steel guide would have caused severe inhomogeneity in the B_0 field as well as causing depolarization of the neutrons in wall collisions. The use of glass also allowed the penetration of the oscillating magnetic field of the spin flip coil, at 20 kHz. This coil was used towards the end of the measurement

cycle, when the spin-down neutrons were emptied from the trap and counted.

To prevent depolarization as the neutrons passed from the magnetic field of the polarizer, through the Earth's $60 \mu\text{T}$ magnetic field, and into the $1 \mu\text{T}$ magnetic field of the trap, a variable-pitch solenoid was wound around an 18-cm-diameter former concentric with the guide tube. This ensured that the magnetic field changed smoothly and monotonically, and that there is no zero-field region along the guide.

3. The neutron storage trap

The neutron storage trap was made of two flat, 30 mm thick, circular aluminum electrodes, separated by a hollow right circular cylinder of quartz that also acted as a high-voltage insulator. The electrodes had aluminum corona domes attached, and the insulator was recessed 15 mm into the electrodes to reduce high-voltage breakdown [70]. At the bottom of the recess in each electrode, a Teflon O-ring was housed to provide a gas-tight seal between the electrode itself and the inner surface of the quartz ring, so as to contain the polarized atomic mercury used for the magnetometry, as described in Section VB.

About halfway through the data-taking period, the existing smooth-walled quartz cylinder was replaced by another quartz cylinder of the same inner dimensions but with a matt surface finish. These are referred to as the smooth and rough traps respectively.

Bare aluminum has a Fermi potential of 55 neV (corresponding to a critical velocity of 3.3 m/s). Aluminum oxide surfaces quickly depolarize any mercury that comes into contact with them. The electrodes are therefore coated with a thin insulating layer of a relatively high Fermi potential material. Initially, Teflon was used for this purpose; it was sprayed on, and baked in an oven. However, it did not adhere well enough to the surface, and it eventually peeled away, causing high-voltage sparks to the resulting loose Teflon flaps. The Teflon was then replaced by a $1 \mu\text{m}$ thick coating of diamond-like carbon (DLC), produced by chemical vapor deposition from a plasma discharge in deuterated methane [71], which proved to be far more durable. The Fermi potential of this layer is 220 neV. The quartz insulator has a Fermi potential of 91 neV. All of the data analysed in this paper were taken with the DLC-coated electrodes.

The trap had an interior diameter of 470 mm and a height of 150 mm. The 15 mm recess in each electrode yielded a distance between the electrodes, for the majority of the surface, of 120 mm. The overall volume was therefore 21 liters.

The annular quartz insulators forming the sidewalls, which were machined from single pieces of fused silica, had a 15 mm wall thickness. A Suprasil window in either side allowed the passage of a beam of polarized 2537 \AA light, which was used to probe the state of polarization

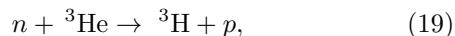
of the mercury atoms as they precessed in the \mathbf{B}_0 field.

The lower electrode was electrically grounded, and had a 67 mm diameter, 4 cm deep hole in the center, through which the neutrons enter the trap. The hole could be closed by a sliding DLC-coated beryllium-copper door that had been adjusted to have gaps of less than 100 μm . This non-magnetic door slid on nylon bearings and it was operated by a mechanical coupling from a remote piston driven by compressed air. A second hole in the electrode, of diameter 10 mm, gave access to a door that opened for 1 s during the measurement cycle to allow the polarized mercury to enter the trap.

The neutron-trap support system, door mechanism, mercury polarizer and all other items inside the vacuum vessel were made from non-ferromagnetic materials. Materials such as brass were avoided because they often contain ferromagnetic impurities. Scans with a fluxgate magnetometer of sensitivity 1 nT approaching to within 2 cm of the inner surface of the storage volume revealed no magnetic anomalies.

4. The neutron detector

The neutron detector was a proportional counter containing 1200 mbar of argon, 50 mbar of ^3He and 100 mbar of methane, in which the neutrons were detected via the reaction



which releases 764 keV of energy. The central electrode was a loop of tungsten wire of diameter 200 μm and was maintained at 2.5 kV [65].

The window of the detector was a 100 μm aluminum foil, with a mean Fermi potential of 55 neV. The detector was placed 2 m below the neutron trap to ensure that nearly all the neutrons reaching it, after falling freely through the Earth's gravitational field, have a sufficiently large velocity component perpendicular to the window to penetrate it. The efficiency of the detector was about 80% for UCN. The detector was shielded by 150 mm of polyethylene and 5 mm of boron-loaded plastic resulting in a background *in situ* of less than one count in 10 s, whereas the average UCN count after a single four-minute measurement cycle was about 14,000 in 40 s for this data set.

B. The mercury magnetometer

The construction and performance [72] of the atomic mercury magnetometer (Fig. 7) have been discussed elsewhere. Here a brief account is given of its use in the EDM experiment.

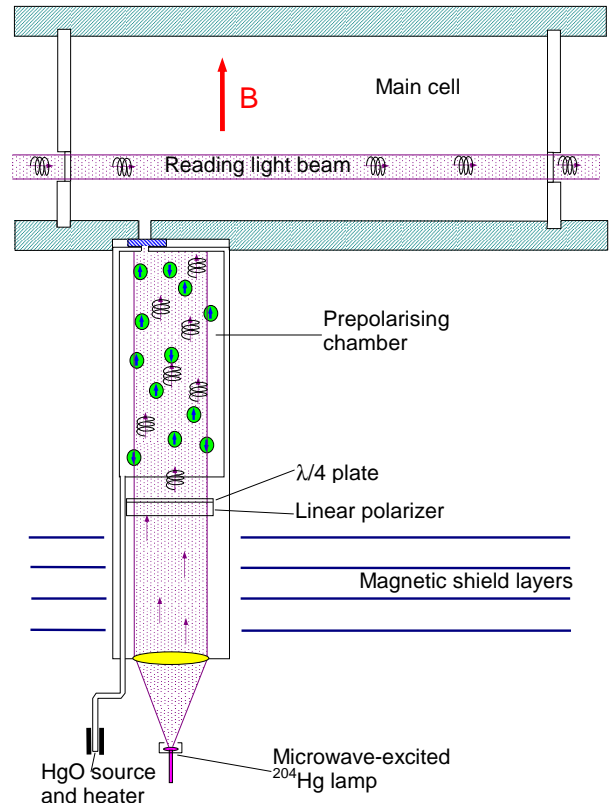


FIG. 7: (Color online) The mercury magnetometer

1. Principle of operation

Spin-polarized ^{199}Hg atoms were made to enter the storage volume once it had been filled with neutrons and the neutron entrance door had been closed. A rotating magnetic field \mathbf{B}'_1 , perpendicular to the main \mathbf{B}_0 field, was applied for a period of 2 s. The \mathbf{B}'_1 field had a frequency equal to the spin precession frequency of the mercury atoms – 7.79 Hz – and was of the appropriate strength to turn the spin polarization vector by $\pi/2$ radians into the xy plane perpendicular to \mathbf{B}_0 . Meanwhile, a beam of 2537 \AA polarized light from an isotopically-pure ^{204}Hg discharge tube traversed the chamber. The absorption of this light depended upon the x component of polarization of the mercury atoms, and thus varied with time as an exponentially-decaying sinusoid. The intensity of the light was monitored by a solar-blind Hamamatsu R431S photomultiplier tube, the output current of which was converted into a voltage and digitised with a 16-bit ADC at a rate of 100 Hz. The resulting data (Fig. 8) were fitted to obtain the average frequency, and hence

the volume- and time-averaged magnetic field, during the Ramsey measurement interval. At the end of the storage period the mercury atoms were pumped out of the cell via the neutron entrance door.

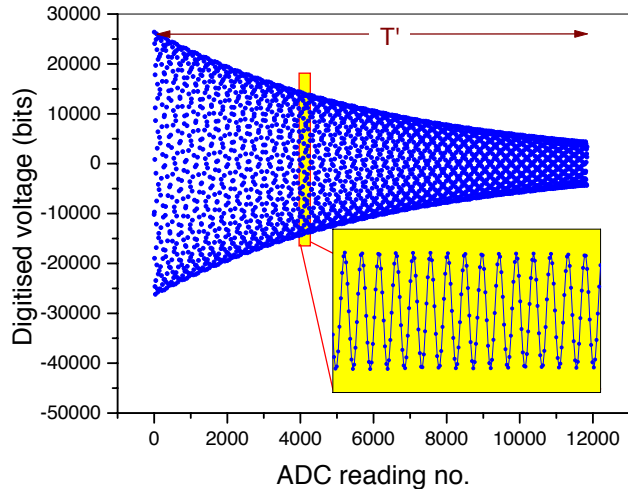


FIG. 8: (Color online) A set of mercury ADC readings from one measurement cycle. The gradual depolarization is clearly visible, and the expanded region shows the underlying 8 Hz precession frequency. The frequency measurement period T' excludes a two-second settling period at the start.

2. Mercury source, polarizer and analyzer

The mercury source was a powder of ^{199}HgO , which was dissociated by continuous heating to approximately 200°C . After passing through a narrow Fomblin-grease coated pipe, the mercury atoms reached a 1.2 liter chamber situated adjacent to the main neutron storage volume, within the $1\ \mu\text{T}$ \mathbf{B}_0 field. There they were optically pumped by light from a ^{204}Hg discharge lamp, identical to that used for monitoring the polarization within the neutron storage volume. The pumping process was continuous, so that, as each charge of polarized atoms entered the storage volume for the frequency measurement, the next charge began to build up and polarize.

The ^{204}Hg discharge lamp lay one focal length below an 80 mm diameter f2 lens (which also served as a vacuum window). The parallel beam of light thus produced passed through a linear polarizer followed by a quarter-wave plate to produce the necessary circular polarization. The analyzing, or reading, light followed a similar arrangement.

3. Absorption and polarization characteristics

The absorption A of the reading light, which was proportional to the number of mercury atoms within the

chamber, is defined as

$$A = \frac{I_0 - I_1}{I_0}, \quad (20)$$

where I_0 and I_1 are the DC levels of the reading light measured just before and just after, respectively, the injection of polarized mercury into the main storage volume. The initial amplitude a of the oscillating signal is related to the polarization P as [72–74]

$$a = I_1 \left\{ (1 - A)^{-P} - 1 \right\}, \quad (21)$$

so the level of polarization may be extracted simply from the absorption and the fitted signal amplitude.

The polarization is found to depend strongly upon A because, in the polarizing chamber, the probability of absorbing a reemitted photon increases quadratically with the density of mercury. Secondary, and higher order, re-absorptions increase even more quickly. A large charge of mercury therefore yields a relatively small polarization. One finds empirically that

$$P \approx p_1 \exp(-A\alpha), \quad (22)$$

where p_1 and α might typically have values of around 0.5 and 6 respectively. The function (21) is maximized at an absorption of approximately 16%, and this therefore provides the optimum signal-to-noise ratio. The temperature of the mercury source was adjusted periodically in order to try to keep the absorption fairly near this value.

4. Calculation of precession frequency

As with other aspects of the magnetometer, the frequency fitting procedure has been discussed in some detail in [72], and it is therefore only briefly described here.

The AC component of the mercury signal was amplified so as to match the input voltage range of the ADC used for its digitisation. The clock pulses that trigger the ADC readings were gated off while the mercury entered the chamber and while the $\pi/2$ pulse was applied, and readings for an additional 2 s after that time were ignored in case they were influenced by transient effects. The readings were, however, recorded throughout the 20 s neutron filling period, during which time there was no mercury in the storage cell. This allowed the evaluation of the rms noise on the signal, from which an estimator of the uncertainty of each reading in the fit could be deduced.

Because the magnetic field drifted with time, the frequency changed slightly during the measurement. Therefore, instead of fitting the entire array of ADC readings to a decaying sinusoid, a pair of shorter ($t = 15$ s) intervals at either end of the Ramsey measurement period were fitted in order to find the phases at points close to the beginning and the end [75]. The total phase difference (including $2n\pi$ for the complete cycles) divided

by the time gives the average frequency, and hence the time- and volume-averaged magnetic field for the interval of free precession.

The fitted function generally appeared to describe the data well, with the χ^2/ν distribution peaking close to 1.0, as shown by the data points in Fig. 9.

The distribution shown in Fig. 9 is truncated at $\chi^2/\nu = 4.5$. If $\chi^2/\nu > 4$, however, the online fitting procedure attempts to correct for potential hardware errors such as missed clock cycles, sticking bits, saturation, too-short depolarisation time, and/or occasional sparks. The discontinuity at 4.0 reflects the fact that the majority of the fits with originally larger χ^2/ν were incorrect, and they have successfully been re-fitted with an appropriate correction for one or more of these problems.

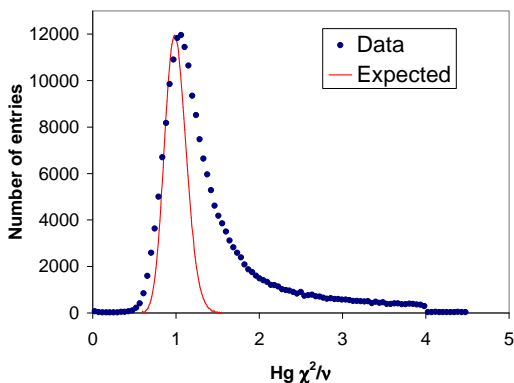


FIG. 9: (Color online) Distribution of χ^2/ν for approximately 205,000 fits of the mercury precession frequency, together with the expected distribution for the ideal case of no magnetic field drift.

5. Effects of the bandpass amplifier

The mercury frequency fitting routine assumed no correlations between the individual ADC readings. The measured rms noise was used as an estimate of the uncertainty of each point. Prior to digitization, however, the mercury signal was filtered by a bandpass amplifier with a Q of approximately 5.9 in order to reduce the noise; consequently, neighbouring ADC measurements are actually rather strongly correlated with one another, and the calculated variance must be modified to allow for this.

If the points were independent, the variance σ^2 of the fitted frequency would be expected to be inversely proportional to the number of readings $n = 3000$ obtained in the short intervals at either end of the signal train, as shown in ref. [72]. When the data are correlated, this is no longer true; for a given bandwidth, increasing the sampling frequency beyond a certain point does not reduce the variance. The calculations in [75] suggest that that point is reached when $n_s Q = 3$, where n_s is the number of readings taken per period. In the case of this

experiment, $n_s = 12.5$ and $Q \approx 5.9$, giving an overall factor of 74, i.e. approximately 25 times above this limit; thus the true variance on the frequency determination is expected to be higher than the naïve estimate by the same factor of 25.

This hypothesis was tested by adding white noise to a precise 8 Hz synthesized signal from a frequency generator, and performing a series of fits of the frequency of the resulting signal, firstly with and then without the bandpass filter in place. With a flat response, the spread in the measured frequencies was consistent with a Gaussian random distribution about the mean, having $\chi^2/\nu = 1.0$. With the bandpass filter, the noise was reduced by a factor of five, as was the estimated uncertainty of each fitted frequency; but the scatter in the results increased, with χ^2/ν rising to 25, suggesting that the error bars were indeed a factor of five too small. Furthermore, this same factor is consistent with the scatter observed in the experimental data during periods when the magnetic field is stable, and it also agrees with estimates based upon numerical simulations using a digital Butterworth filter.

In the discussions that follow, all calculated uncertainties in the mercury precession frequency incorporate a factor of 5.0 (i.e., a factor of 25 in the variance) to allow for this narrow-banding effect.

This same effect also broadens the χ^2/ν distribution. The expected distribution, shown as a smooth curve in Fig. 9, is therefore that appropriate to $3000/25 = 120$ degrees of freedom. As the magnetic field during each measurement period drifts slightly, the frequency is not perfectly constant. The true distribution is therefore expected to broaden further, particularly on the high side. There is a reasonable match on the low side, and the position of the peak is close to unity.

6. Performance of the magnetometer

As with the neutrons, it is desirable that the absolute precision of the mercury frequency measurements should be better than 0.2 ppm. In Section VB11 we discuss possible mechanisms that could affect the accuracy of this system.

Fig. 10 shows a typical example of the evolution of the magnetic field, as measured by the mercury precession frequency, throughout a typical run. Error bars, which are of the order of a microhertz, are smaller than the points themselves on this plot. The drift in magnetic field during this time is approximately 5×10^{-11} T. For this run an electric field of magnitude 4 kV/cm was applied to the storage volume, with its polarity reversing approximately every 70 minutes.

Fig. 11 shows the corresponding series of measurements of the neutron resonant frequency throughout the same 26-hour period. As expected, the same drift in magnetic field is reflected in this set of data. Error bars are again omitted for clarity, but are of order $29 \mu\text{Hz}$ for this particular data set. The ratio of neutron to mercury

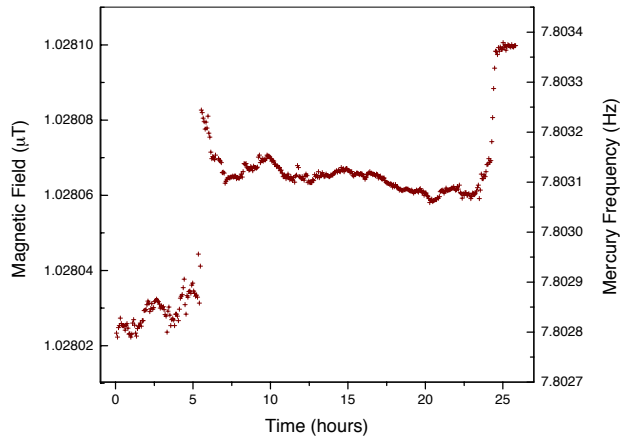


FIG. 10: (Color online) Magnetic field strength, as determined by the mercury resonant frequency, measured repeatedly over a 26-hour period.

frequencies, normalised to the mean neutron frequency — i.e., the measured neutron frequency corrected for the magnetic field drift — is shown on the same plot, where it appears as a flat line. The uncertainty on each point is approximately one part per million, giving a χ^2/ν of 0.89; this is consistent with the width of the line being entirely dominated by neutron counting statistics. Any change in the neutron resonant frequency due to the interaction of the electric field with the neutron EDM would appear as a change in this ratio of frequencies. A straight-line fit to the ratio as a function of the applied electric field therefore yields a slope that is directly proportional to the EDM signal. It is evident that the use of this magnetometer compensates extremely efficiently for the large-scale effects of magnetic-field drift.

7. Mercury frequency uncertainty

The fitted Hg frequency sometimes has a relatively large uncertainty, particularly if the depolarization time is short. The distribution of these uncertainties is shown in Fig. 12; a typical value is 1-2 μHz . For comparison, the typical inherent neutron frequency uncertainty from counting statistics was about 20 μHz , corresponding to about 5 μHz in the mercury system.

8. Magnetic field jumps

The distribution of Hg frequency jumps, i.e. the difference in Hg frequency between a given batch and the previous batch, is shown in Fig. 13. There are broad tails due to occasional sudden changes in field, for example due to the movement of an overhead crane or to a mechanical disturbance to the μ -metal shields.

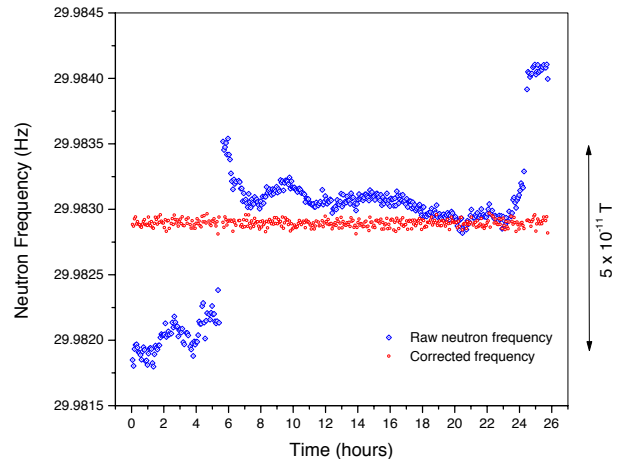


FIG. 11: (Color online) Neutron resonant frequency, measured over the same 26-hour period, before and after correction of the effect of the drifting magnetic field by normalisation to the measurements of the mercury magnetometer.

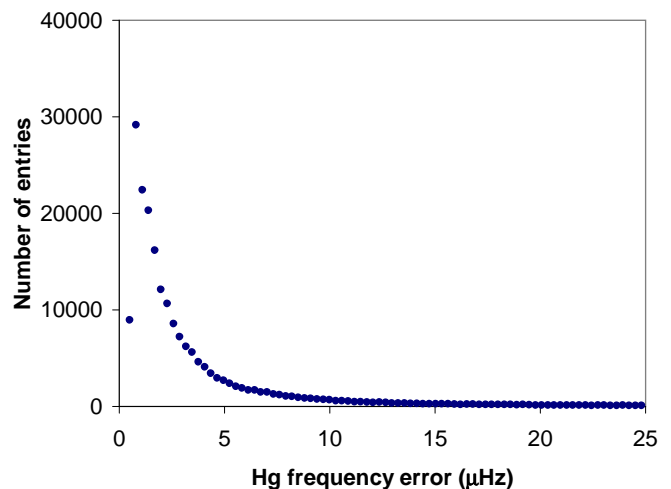


FIG. 12: (Color online) Distribution of uncertainties of the fitted Hg precession frequency

The mercury and the neutron frequency measurements do not have perfect temporal overlap. One can consider the start and end of the Hg measurements to be centred on the 15-second averaging period at the start and end of the Ramsey measurement time, whereas the neutrons average over all but 2 seconds at either end. If the field is changing, there is therefore a roughly 7-second period — i.e. about 1/30 of the total batch period — for which the change is not properly accounted. For comparison, a frequency jump of 60 μHz — which would be regarded as extreme — corresponds to a field jump of about 7.5 ppm, or just over 1/20 of the Ramsey linewidth. With the aforementioned protection factor of 1/30, this cor-

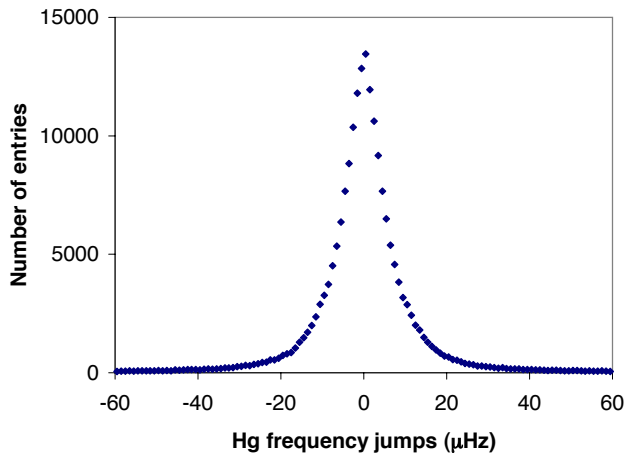


FIG. 13: (Color online) Distribution of changes in the Hg frequency from one batch cycle to the next

responds to a potential error in the frequency ratio R of 0.25 ppm, to be compared with a typical statistical uncertainty on the neutron frequency of about 0.7 ppm.

9. Depolarization in strong electric fields

The depolarization time of the mercury depended strongly upon the high voltage behavior of the storage cell. As the upper electrode was charged up, the mercury depolarization time dropped precipitously, after which it slowly recovered over a timescale of about an hour. Discharging and recharging at the same polarity had little effect, but charging at the opposite polarity once again shortened the depolarization time. During a normal EDM run, the polarity was reversed about once per hour. The depolarization times therefore followed a characteristic pattern of a series of rapid falls followed by slow recoveries, upon which was superimposed a gradual overall reduction, as shown in Fig. 14. Sparks also caused a rapid depolarization, from which there was only partial recovery.

This effect of a temporary increase in relaxation each time the HV polarity is reversed may be due to protons (H^+ ions) appearing on the newly positive electrode. Electron migration in the dielectric surface layer soon takes over, and the protons diffuse back into the surface layers again with a characteristic \sqrt{t} dependence as the HT dwell progresses. Protons are believed to catalyse the mercury depolarisation by forming the paramagnetic short-lived (10^{-6} s) HgH molecules in surface encounters.

The depolarization time could be restored to a large extent by a high-voltage discharge in 1 torr of oxygen; it was normally necessary to carry out this procedure every 1-3 days. Prior to this cleaning, the system was usually “trained” by increasing the voltage to a fairly high value (between 120 and 170 kV) and allowing it to settle until

it could stay for several minutes without discharging, as discussed in Section VD below. Cleaning the quartz ring and then heating it in 10^{-2} torr of He at 60 °C for about two days was also beneficial to the depolarization time; this procedure was carried out between reactor cycles.

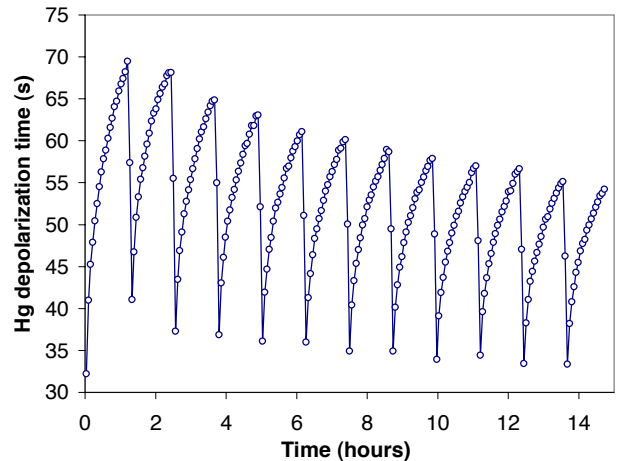


FIG. 14: (Color online) Behavior of the mercury depolarization time during repeated reversal of the applied electric field.

This detrimental effect of the high voltage upon the mercury depolarization time could result in a false EDM signal if (a) the average depolarization time were different for the two HV polarities, and (b) the mercury frequency had some small dependence upon the depolarization time. The cycle-by-cycle dependence of the neutron-to-mercury frequency ratio R upon the mercury depolarization time τ was found to be $\partial R/\partial \tau = (-0.5 \pm 3.2) \times 10^{-4}$ ppm per second for negative HV and $(+2.2 \pm 3.3) \times 10^{-4}$ ppm per second for positive HV, with an overall average of $(+0.9 \pm 2.3) \times 10^{-4}$ ppm per second. Coupled with a difference in average depolarization times (where the average has been calculated by weighting with the EDM measurement uncertainties) of $\tau_- - \tau_+ = 2.0 \pm 0.2$ s, an average effective neutron frequency shift above 12 nHz may be excluded at 90% CL. Such a frequency shift might conceivably contribute a false EDM signal of up to 1.2×10^{-27} e cm. However, this effect will cancel upon reversal of the magnetic field. As the quantities of data (as measured by the statistical uncertainty) for the two field directions were identical to within 1%, an error from this source is excluded at the level of 1.2×10^{-29} e cm.

This behavior of the mercury strongly constrained the sensitivity of the experiment, as it limited the magnitude of the electric field to a value substantially below the limit that could be set by leakage currents alone.

10. Mercury light shift

The presence of the Hg reading light, via the Ramsey-Bloch-Siegert mechanism [60, 61], shifts the resonant frequency of the Hg atoms. These so-called light shifts are produced [76, 77] by any small component, parallel to \mathbf{B}_0 , of the ^{204}Hg probe light beam passing through the precessing ^{199}Hg atoms. This component, and the consequent shift in the neutron-to-mercury frequency ratio R , reverse sign on reversal of \mathbf{B}_0 . A slight dependence of R on the incident light intensity was indeed observed in this apparatus, the magnitude ~ 0.2 ppm being in agreement with theory. Any changes in intensity correlated with the electric field direction would then result in a frequency shift that would mimic an EDM. This is the so-called direct light shift discussed in [1]. It is possible to modify the optics to reduce the amount of light travelling in the direction parallel to B_0 , and in fact this has recently been carried out by the current users of this apparatus.

The method of establishing the light-intensity dependence was as follows. The reading-light beam can contain several different wavelength components, only one of which serves to measure the ^{199}Hg precession. The raw intensity I_0 of the light cannot therefore be used to measure any effect of intensity upon R . Instead, the amplitude a of the AC component of the light was used; but it was necessary first to correct it for absorption. The amplitude as a function of absorption has a characteristic shape that peaks at approximately 16% absorption over a wide range of light intensities. It was therefore possible to adjust the measured a for each batch cycle within a run in order to bring it back to its peak value, i.e. the value a_{16} that it would have at 16% absorption.

The signal amplitude as a function of the absorption A and polarization P is approximately [72] (c.f. Eq. 20)

$$a = I_0 (1 - A) \left\{ (1 - A)^{-P} - 1 \right\}. \quad (23)$$

This analysis was restricted to polarizations between 5% and 40%, and to absorptions greater than 5%, for which this parameterization is appropriate.

The polarization achieved depends upon the quantity of ^{199}Hg within the trap, due to the relaxing effect of reemitted photons: the probability of absorbing a reemitted photon increases linearly with the Hg density. Secondary (and higher) reabsorptions increase even more quickly. In consequence, P has an exponential dependence upon A :

$$P = P_0 e^{-A/A_0}. \quad (24)$$

Fitting this function within each run yields a characteristic value P_{16} for the polarisation that corresponds to 16% absorption. The absorption-corrected amplitude a_{16} for any A and P within that run is then given by

$$a_{16} = a \frac{0.84 (0.84^{-P_{16}} - 1)}{(1 - A) \{ (1 - A)^{-P} - 1 \}}. \quad (25)$$

A linear dependence of R on a_{16} was fitted for each run. Over the six-year period of data taking for which this apparatus was used, two separate neutron traps were used: one had a rough wall, the other smooth. A weighted average of the resulting slopes was calculated for each of these two traps and for each direction of \mathbf{B}_0 .

An effect of this kind, if present, is expected to be of the order of a fraction of a part per million and is expected to change sign upon reversal of \mathbf{B}_0 . The consistency of observed results suggested that it was appropriate to average the results from the two field directions, to obtain a magnitude of 0.21 ± 0.08 ppm/V for the rough trap. The results for the smooth trap, 0.01 ± 0.03 ppm/V, were consistent with zero. It was then possible to correct the rough-trap data for this effect on a run-by-run basis, using the average a_{16} for the run in question.

The amplitude a_{16} was also observed to have a slight dependence upon the applied HV, as follows:

- For \mathbf{B}_0 up: $\partial a_{16}/\partial V = 4.7 \pm 1.2 \times 10^{-6}$ volts per kV of applied HV
- For \mathbf{B}_0 down: $\partial a_{16}/\partial V = 11.0 \pm 1.6 \times 10^{-6}$ volts per kV of applied HV
- Average: $\partial a_{16}/\partial V = 8 \pm 1 \times 10^{-6}$ volts per kV.

However, since it is possible to correct this dependence to within its uncertainty, no net bias should be expected from this source. There remains an uncertainty on the dependence of R on the HV of $(\partial a_{16}/\partial V) \times (\partial R/\partial a_{16}) = 3 \times 10^{-7}$ ppm per applied kV when averaged over both data-taking traps. The light-signal amplitude dependence on HV is independent of the sign of \mathbf{B}_0 , but the light-induced frequency shift does change sign with \mathbf{B} , and this effect will therefore not cancel upon reversal of \mathbf{B}_0 . For a trap of height $H = 12$ cm this effect therefore contributes an uncertainty of

$$\frac{h}{2} \frac{\partial \nu}{\partial E} = \frac{h\nu}{2} \frac{\partial R}{\partial V} H = 2 \times 10^{-28} e \text{ cm}. \quad (26)$$

11. Accuracy of Hg frequency measurements

A number of mechanisms can affect the frequency measurement of the Hg magnetometer. Although these do not necessarily have a direct impact upon the EDM measurement, we summarize them here for completeness.

First, an analog of the Bloch-Siegert-Ramsey shift is the light shift due to virtual transitions caused by the probe light beam. The size of this effect is estimated to be 0.15 ppm, both by calculations from first principles and as assessed in the data by looking for frequency versus light intensity correlations: the latter analysis was used, as described above, to correct for this shift.

Next, there is a real transition shift caused by the fact that about 10 % of the Hg atoms used to measure the final phase have been excited once before. In the excited state they precess backwards through about 1° , and some

of the polarization survives the excitation and decay. The effect is as though the gyromagnetic factor and precession frequency were reduced by 0.1 ppm in the auxiliary trap and by 0.25 ppm in the data-taking trap. These shifts are expected to be completely unchanged by the reversal of B_0 .

The total Hg absorption of the light beam is typically 15%, which gives us a nearly optimum signal-to-noise ratio. Each atom that absorbs a photon is depolarized after the subsequent spontaneous decay ($\tau = 1.2 \times 10^{-7}$ s). The ensemble spin depolarization rate from this cause is about 1/1800 s. The typical observed total spin depolarization rate is 1/60 s. The contribution from magnetic-field inhomogeneity is expected to be about a hundred times less than that of the neutrons (1/600s) making it a negligible 1/60000 s. The dominant relaxation rate, close to 1/60 s, is due to spin relaxation when the Hg atoms stick on the wall.

The Hg initial phase is established by the two-second 90° spin-flip using a rotating field at 8 Hz. Each Hg atom makes about 2000 free paths in the trap during the spin-flip, so the phase information is very uniformly implanted over the trap volume. It continues to become more and more uniformly spread by the Hg motion while the neutrons are flipped using rf at 30 Hz. The initial Hg phase is then sampled on the basis of the 1% of Hg atoms that absorb a photon from the light beam during the next 15 s. (These atoms are partly depolarized in the process.) The final Hg phase is determined from the Hg atoms that absorb a photon in the last 15 seconds before the second UCN spin flip. There are a number of reasons why the Hg frequency, thus determined, does not represent a perfect volume average of the field:

1. Finite volume of the light beam: For all the Hg atoms that absorb a photon to measure the final phase, the last 1 millisecond of trajectory must certainly be near the light beam. This creates a phase bias. The B_0 field near the light could be different by 10^{-3} fractional compared with the volume average. This is 0.01 ppm of the total phase previously accumulated. The bias should be the same both for the initial and final phase measurements, so that it cancels out. The overall shift is expected to be less than 0.001 ppm.
2. Artefacts: The system of determining the frequency in the light detector signal has been tested at the 0.1 ppm level by feeding in sine waves from the frequency synthesiser.
3. Bias from Hg atoms dwelling on the wall: Free path transits take about 10^{-3} s. The sticking time on the wall is thought to be about 10^{-8} s. Thus, the overall average has a surface average weighting of 10^{-5} compared to the volume average. The surface average value of B_z may differ by one part per thousand from the volume average, causing an overall error of about 0.01 ppm.

4. Bias due to surface relaxation or differential loss: This may occur if the relaxation is faster on one wall than another, or if there is a loss of atoms preferentially at one end of the cell. Suppose, for example, that the roof has an excess relaxation rate of 1/100 s compared with the other surfaces. Each atom is colliding at about 1000 Hz, of which 250 Hz is on the roof. The probability of depolarization per roof collision is thus $P = 4 \times 10^{-5}$. We have analysed this problem and find that a shift occurs in the centre of measurement. Under the most pessimistic assumptions the shift Δh can reach the value $(H/8)P$, where H is the trap height – in this case, $(5 \times 10^{-6})H$, or 6×10^{-4} mm. When the magnetic field is not trimmed, the maximum $\partial B_z/\partial z$ gradients are 10^{-5} fractional per mm, or 1 nT/10 cm. The systematic bias from Δh is thus 0.006 ppm.
5. False EDM due to surface relaxation: The temporary increase in relaxation observed each time the HV polarity is reversed has been discussed above. This process swings some of the depolarisation rate backwards and forwards from roof to floor in synchronism with the HV polarity change. This can create a false EDM signal via a finite $\partial B_z/\partial z$. The transient partial relaxation rate averaged over an HT dwell is observed to be about 1/100 s, making a displacement of 6×10^{-4} mm. In the case of a $\partial B_z/\partial z$ gradient of 0.35 ppm/mm (corresponding to an R_a shift of 1 ppm), the systematic false field change seen by the Hg magnetometer is about 2×10^{-4} ppm or 2×10^{-16} T. This corresponds to a false EDM of about 2×10^{-27} e cm, some 1/20th of the geometric-phase false EDM. In practice it would have the same signature as the geometric phase false EDM, being proportional to R_a and changing sign with the direction of B_0 . It would simply act to increase the gradient of both data lines by about 5%. Currently the lines have a fitted gradient that is 20% \pm 15% above the GP phase theoretical prediction. This additional effect could easily be present. All of its consequences have been covered by our GP corrections.
6. Finally, variation of light intensity with HV has been dealt with above. If there were preferential depolarization of Hg on, say, the positive electrode, thus biasing the volume-averaged frequency measurement, it could slightly alter the gradients of the lines in Fig. 2 of [1], similarly to other gradient-changing mechanisms listed; but again, it is not a cause for concern as it does not affect the outcome of the analysis.

C. The magnetic field

To carry out a magnetic resonance experiment one must impose conditions on both the homogeneity and the time stability of the magnetic field: the field must be sufficiently homogeneous to retain polarization of the neutrons until the end of the storage time, and it should be sufficiently stable so as not to increase significantly the uncertainty in the determination of the precession frequency beyond that due to neutron counting statistics.

1. The magnetic shield

In the environment of the experimental area magnetic field changes of up to 1 μT in a few tens of seconds are quite common, and are often associated with movements of the reactor crane, or with the operation of magnetic spectrometers. To provide the required homogeneity and stability of the magnetic field, the neutron storage volume was set inside a four-layer μ -metal magnetic shield. The dimensions of the magnetic shield layers are given in Table I. The two inner layers and their detachable endcaps had welded joints, and were annealed in a reducing hydrazine (N_2H_4) atmosphere at 1050 $^\circ\text{C}$ after manufacture [78]. The two outer layers, which were too large to have been fired in a single piece, were made from sheets of μ -metal individually annealed and bolted together with 150 mm overlaps. All four layers had 210 mm diameter holes at the top and bottom of the mid-plane of the central cylinder: The bottom hole contained the neutron guide tube, and the top contained the high-voltage feedthrough. The endcaps of the innermost layer had a 45 mm hole in the center, and each of the other three layers had a 32 mm hole. Originally, the apparatus had been built with a fifth, innermost, layer of shielding, which was removed in the meantime to allow for enlargement of the storage vessel. The shielding factor for the set of five shields was measured by winding a pair of coils around the external shield frame and measuring the magnetic field change at the center of the shields with three rubidium magnetometers. The dynamic shielding factor to external magnetic field changes was found to be approximately 2×10^5 radially and 2×10^4 axially [79]. With the four-layer shield, the shielding factor transverse to the axis is approximately 1.5×10^4 , consistent with expectation and also with comparisons made between changing external fields and changes registered by the mercury magnetometer.

2. The magnetic field coil

The coil to generate the 1 μT static magnetic field \mathbf{B}_0 was wound and glued directly onto the aluminum vacuum vessel. The coil fitted snugly inside the innermost layer of

Shield	R (m)	l_1 (m)	l_2 (m)	Overlap (m)	t (mm)
1	0.97	2.74	2.74	0.20	1.5
2	0.79	2.30	2.30	0.20	1.5
3	0.68	0.75	1.89	0.12	2.0
4	0.58	0.75	1.63	0.12	2.0

TABLE I: The dimensions of the four-layer magnetic shield. Each layer consisted of a central cylinder, of radius R and length l_1 , and two detachable endcaps. The length l_2 is that of the central cylinder plus the endcaps, when assembled. The overlap is the distance by which the endcaps overlapped the central cylinders. t is the thickness of the μ -metal used in both the central cylinders and the endcaps.

the magnetic shield and was wound with a $\cos\theta$ distribution to give a constant number of turns per unit distance along the vertical diameter of the cylinder. Theoretically a coil of constant pitch wound on the surface of a cavity inside a material of infinite permeability produces a homogeneous magnetic field, regardless of variation in the cross-sectional area of the cavity. The coil winding used here was an approximation to this ideal state. The turns were wound 20 mm apart, and access to the neutron trap required breaking all of the turns in order to remove the end of the cylinder. Every turn on the coil, therefore, had two breaks on each end face of the cylinder, where the electrical connection was made with a brass screw and two brass solder tags. The magnetic field was aligned with the vertical diameter of the cylindrical shield, rather than along the axis, to take advantage of the fact that the radial magnetic shielding factor is greater than the axial shielding factor.

The choice for the magnitude of \mathbf{B}_0 was arbitrary, in the sense that it does not enter directly into the expression for the sensitivity of the experiment. There are, however, a number of other factors that had a strong bearing on the choice, *viz*: the field should be large compared to any residual fields inside the trap (≤ 2 nT), so that the axis of quantization for the neutrons, which is determined by \mathbf{B}_0 , is in the same direction everywhere; the field should be large enough to prevent depolarization of the neutrons as they pass into the shields; the homogeneity requirements given below must be fulfilled (in general, field gradients increase linearly with the field itself, thus placing a limit on the maximum field); the field should be as stable as possible, which is generally easier to achieve at lower fields; and finally, it was desirable to keep the precession frequency away from the 50 Hz mains frequency. The 1 μT magnetic field chosen in this case gave a resonant frequency of about 30 Hz for the neutrons.

The coil that generated the \mathbf{B}_0 field had a resistance of approximately 10 Ω , and required a current of 17 mA to provide the 1 μT field. The stabilizer providing this current contained a precision voltage reference with a very low output voltage temperature coefficient (National Semiconductors LM169B; 1 ppm/ $^\circ\text{C}$) and an operational amplifier with a very low input offset voltage temperature

coefficient (Analog Devices OP177A; $0.03\mu\text{V}/^\circ\text{C}$). High-stability precision wire-wound resistors ($3\text{ ppm}/^\circ\text{C}$) were used to define the \mathbf{B}_0 field current. High thermal conductivity resin was used to connect the components to the inside of a cylindrical aluminum block (approximately 100 mm in diameter and 100 mm long). This block, which acted as a heat reservoir for the temperature-critical components, was thermally isolated from the surroundings and from the power supply by more than 100 mm of polystyrene foam. The average electrical potential of the coil was maintained at the same potential as the vacuum tank upon which it was wound, in order to minimize currents to the coil supports.

3. Homogeneity

The homogeneity requirement for a magnetic resonance experiment in a low-field region is given by Ramsey [80], following the theory of the hydrogen maser [81]. Consider the neutron storage volume to be characterized by a length l and to consist of two regions of magnetic field that differ by ΔB . If $\gamma = -2\mu_n/\hbar$ is the gyromagnetic ratio, then neutrons with velocity v passing from one field region to the other experience a relative phase shift of

$$\delta\phi = \gamma\Delta B l/v. \quad (27)$$

In a storage time T_s , the neutron will experience $M = vT_s/l$ such phase shifts, which will add randomly, so that the phase spread during the storage time is

$$\Delta\phi \approx \delta\phi\sqrt{M} = \gamma\Delta B\sqrt{lT_s/v}. \quad (28)$$

At the end of the storage time $\Delta\phi$ represents the typical phase difference between any two neutrons arising from them having followed different paths across the trap. Maintaining polarization requires that $\Delta\phi < 1$, from which arises the homogeneity constraint

$$\Delta B_0 < \frac{1}{\gamma}\sqrt{\frac{v}{lT_s}}. \quad (29)$$

It should be noted that it is the absolute inhomogeneity of the field ΔB_0 that is constrained, and not the relative homogeneity $\Delta B_0/B_0$. Taking $v = 5\text{ ms}^{-1}$, $l = 150\text{ mm}$, $T_s = 150\text{ s}$ and $\gamma = 1.8 \times 10^8\text{ radians s}^{-1}\text{ T}^{-1}$, the limit becomes $\Delta B_0 < 3\text{ nT}$. For a B_0 field of $1\text{ }\mu\text{T}$ this requires a relative homogeneity of $\Delta B_0/B_0 < 3 \times 10^{-3}$ over the 20-liter neutron storage volume.

The magnetic field within the storage volume was mapped using a three-axis fluxgate magnetometer probe [82]. Spatial variations were found to be of the order of the $\approx 1\text{ nT}$ resolution of the instrument, as long as the shield was demagnetized each time that the magnetic field configuration changed (i.e., each time the magnetic shield was opened or the direction of \mathbf{B}_0 was reversed). Demagnetization was carried out by using a current loop

that was threaded through all of the shields, parallel to the cylinder axis. The current was initially set to 100 ampère-turns, reversed every 2 s and steadily reduced to zero over twenty minutes. Trim coils were used to achieve this level of homogeneity; without them, the field variations would have been about four times greater. The T_2 neutron polarization relaxation time was typically about 600 s; the field inside the trap was therefore adequately homogeneous to meet the requirements of the experiment.

4. Stability

In order to ensure that any noise on the EDM signal caused by magnetic field instabilities was significantly less than that due to neutron counting statistics, it was required that the shift in precession frequency between consecutive measurements should normally be not much larger than the uncertainty due to neutron counting statistics. Thus,

$$\left| \frac{dB_0}{dt} \right| \frac{\gamma T_s}{2\pi} \lesssim \frac{1}{2\pi\alpha T_s \sqrt{N}}. \quad (30)$$

For $\alpha = 0.5$, $T_s = 130\text{ s}$, and $N = 10\,000$ the constraint therefore becomes $|dB_0/dt| \lesssim 8\text{ fT/s}$. For $B_0 = 1\text{ }\mu\text{T}$, this requires a stability of about one part per million over 130 s. However, this criterion is stricter than was necessary in this instance, for two reasons. First, the separated oscillating field method itself is relatively insensitive to fluctuations in the magnetic field on time scales short compared with T_s . This is because the neutron counts are determined by the total accumulated phase difference between the neutron polarization and the oscillator, and not by a detailed comparison throughout the storage cycle. Second, the measured mercury precession frequency was used for normalisation. Except for a period of about 5% at either end of the storage time, any drifting of the magnetic field affected both spin systems in exactly the same manner, and averaging over the entire Ramsey measurement period reduced the influence of any changes that did occur during the end mismatch periods by an order of magnitude. In practice, though, condition (30) was usually satisfied. On the rare occasions when the field changed much more rapidly than this, the mercury precession was generally disturbed to such an extent that χ^2/ν for the frequency fit became extremely large, and the data point was rejected.

5. Uncompensated magnetic field fluctuations

In principle it is possible to have residual effects from \mathbf{B} field fluctuations, such as hysteresis in the μ -metal shield following disturbances in the stabilised \mathbf{B}_0 coil current supply caused by pickup from the high voltage changes. This would manifest itself most strongly as a dipole-like

field \mathbf{B}_d originating from the μ -metal in the region of the HV feedthrough, which would be sensed by both the neutrons and the mercury magnetometer but with a difference given by $\delta B_d/B_d = 3\Delta h/r$ where $r \sim 55$ cm is the distance from the source of the field to the center of the trap. Thus, fluctuations in \mathbf{B} that are correlated with the HV can be expected to be compensated up to a factor of about 70. In order to study this, the mercury and neutron channels were analysed independently.

The analysis was performed by selecting sequences of measurement cycles within each run for which the magnetic field (as measured by the mercury frequency) varied smoothly throughout several high-voltage dwell periods. Both the mercury and the neutron frequencies for each such sequence were fitted to a low-order polynomial. The fits were unweighted, since the displacement from the fitted function was entirely dominated by the magnetic fluctuations rather than by the uncertainties in the frequency calculation associated with each point. The residuals were then fitted to a linear function of the applied electric field to yield the apparent EDM measurements. A plot of the neutron vs. the Hg results (Fig. 15) shows complete (within uncertainties) correlation between the results, with the slope of the best-fit line (-3.83 ± 0.08) corresponding as expected to the ratio of gyromagnetic ratios.

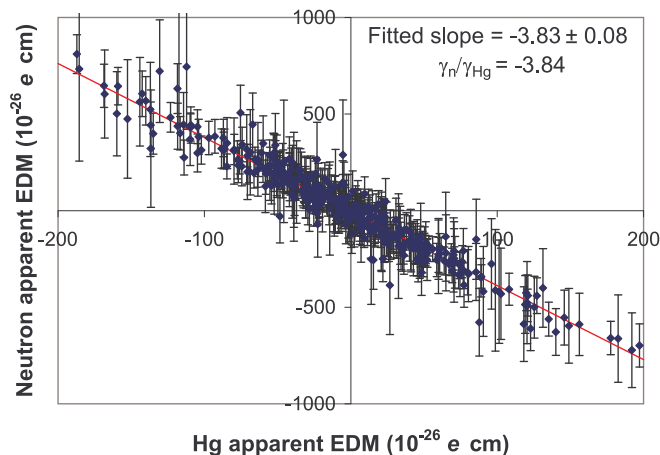


FIG. 15: (Color online) Apparent neutron EDM signals (due to uncompensated random magnetic field fluctuations) as a function of the corresponding apparent mercury EDM signals.

The neutrons yielded a net uncompensated EDM signal of $(17 \pm 4) \times 10^{-26}$ e cm; the Hg (once geometric-phase-induced false EDM contributions[49] had been subtracted) yielded $(-3.9 \pm 0.8) \times 10^{-26}$ e cm. These results are consistent with a common source of magnetic fluctuations correlated with the HV. We therefore expect the mercury-magnetometer compensation to shield us from this systematic effect to a level of $17 \times 10^{-26}/70 = 2.4 \times 10^{-27}$ e cm.

D. The electric field

The main requirements for the electric field were that it should be as large as possible and aligned with the magnetic field, but with the constraint that the leakage current through the insulator of the neutron trap should not generally exceed a few nanoamps. This latter restriction arises because the magnetic fields produced by currents circulating around the trap would induce shifts in the precession frequency that were correlated with the electric field. Although such frequency shifts would be compensated to the level of at least 90% by the mercury magnetometer, any residual effect could result in a systematic error in the EDM, as discussed below.

Sparks could also in principle generate a systematic effect if they changed the magnetization of the shields and if they occurred preferentially for one polarity of the electric field. However, the mercury magnetometer would naturally compensate for any such effect, just as with any other shifts in the magnetic field.

Sparks were also undesirable because, as discussed in Section (VB9) above, they caused the mercury atoms to depolarize rapidly. The frequency at which sparks occurred depended upon the voltage used, the quality of the vacuum, and the conditioning of the system [70]. Sparks occurred more frequently when the experiment was under vacuum ($\approx 10^{-6}$ torr) than they did when a pressure of 10^{-3} torr of either dry nitrogen or helium was maintained in the system. Helium was found to be more efficient than nitrogen in quenching sparks.

Before the start of each data run, the electric field was raised as far as possible (typically 1.5 MVm $^{-1}$), maintained for several minutes, and then lowered and applied with the opposite polarity. This was repeated several times. The effect was to reduce both the quiescent current across the trap and to suppress almost entirely the occurrence of sparks during normal data taking. It was then necessary to “clean” the trap with a short high-voltage discharge in 1 torr of O $_2$ (with a current of 130 μ A for approximately two minutes at each polarity, twice) in order to restore the depolarization time of the mercury to a reasonable value. To some extent the cleaning reverses the beneficial effects of the training, and so the cleaning period is kept as brief as possible. The maximum electric field used for data taking was 1 MV m $^{-1}$, since occasional high-voltage breakdowns tended to occur beyond this limit, resulting in a reduction in the mercury depolarization time.

As sparks invariably disrupt the mercury frequency measurement, batch cycles that contain them are excluded from the analysis, so beyond the residual effects just discussed the sparks themselves cannot contribute to any artificial EDM signals.

1. The high-voltage stack

The electric field was generated by a reversible Cockcroft-Walton type high voltage stack, shown schematically in Fig. 16. The stack was powered by a controller from Bonar Wallis [83].

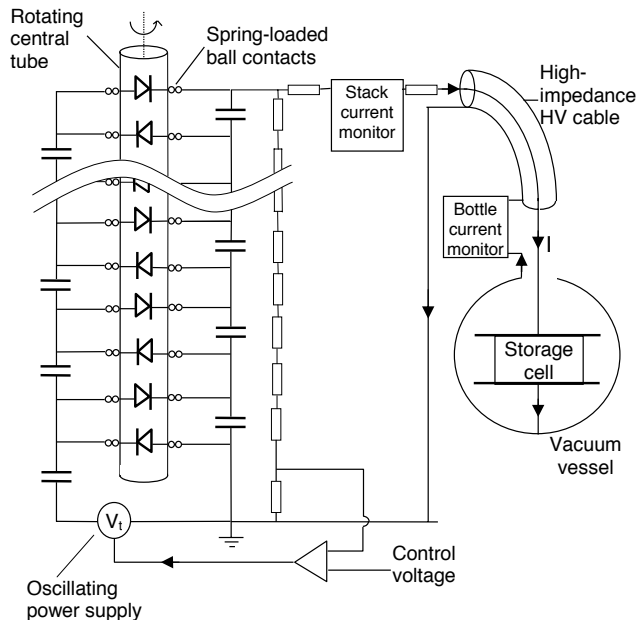


FIG. 16: The reversible Cockcroft-Walton type high-voltage stack, and the current path through the EDM apparatus.

The polarity of the electric field within the neutron trap was reversed by changing the sign of the voltage applied to the ungrounded electrode. This was done by physically reversing the diodes in the charging stack, with the stack at zero voltage. The reversal was driven, under computer control, by a 180° rotation of the core of the stack using compressed air. The stack was connected to the neutron trap by 5 m of coaxial high-voltage cable with its central conductor removed and replaced with oil. A semiconducting sheath around the central conductor remained, and this provided the primary conducting path through the cable. There was a $1 \text{ G}\Omega$ resistance in series between the cable and the trap, to limit the current.

The stack, which was capable of providing $\pm 300 \text{ kV}$, was driven by a 20 kHz oscillator connected to the lowest of its 15 stages. Each stage was separated from its neighbors by a 3.6 nF capacitor, and a return current through a $2.8 \text{ G}\Omega$ resistor chain from the top stage was used by the controller to stabilise the output voltage.

2. Monitoring the high voltage

The electric field in the trap was monitored by recording the magnitude and sign of the voltage at the top of

the stack, the current flowing through the stack, and the current in the feedthrough just above the trap, which charged up the electrodes (primarily displacement current) as the electric field was changed. Fig. 16 shows schematically how the current through the neutron trap was monitored. The coaxial arrangement of the trap and the return current path ensured that the magnetic effects of this current were minimized. This design arose from the experience gained in the earliest version of this experiment: At that time, the vacuum vessel was a glass jar, and no coaxial return current path was available. Sparks within the experimental apparatus were then seen to magnetize the shields permanently, producing changes of as much as 1 mHz in the precession frequency of the neutrons. With the arrangement described here no such effects were seen in this experiment.

3. Leakage currents and their effects

By a suitable choice of the high-voltage setting the quiescent current through the trap was typically kept at or below a few nA. The distribution for both polarities is shown in Fig. 17.

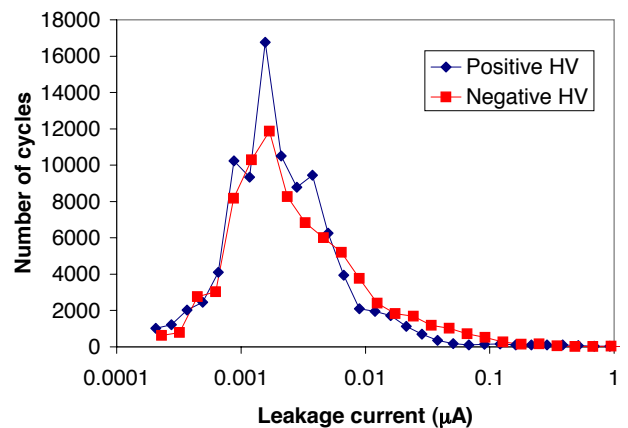


FIG. 17: (Color online) Distribution of the average leakage currents observed during each batch cycle. I

If the current flows in an axial direction through (or along the surface of) the insulator between the electrodes, the magnetic field that it produces will be at right angles to \vec{B}_0 . This field will be small compared with \vec{B}_0 and will produce a shift in the precession frequency that is independent of the polarity of the electric field; thus, this will not be a source of error in the measurement of the EDM. However, one cannot assume that the current will take such a direct path. The insulator is likely to contain paths of different resistances, which could lead to the current having a net azimuthal component. (The insulator ring showed some mild discoloration indicating the path of discharges along its surface. For the most part these

were vertical, but occasionally they were at an angle of up to 45° . It is likely that discharges along the surface of the insulator occurred most often in the vicinity of the windows for the mercury light.) In this case, a component of the magnetic field due to the current would be parallel (or anti-parallel) to \vec{B}_0 and would produce a frequency shift that changes sign when the polarity of the electric field is reversed, giving rise to a systematic error in the EDM. This effect can be estimated for the case in which the current I makes a fraction f of a complete turn around the insulator. If the insulator has radius r , the magnetic field at the center of this current loop is

$$B = \frac{\mu_0 I}{2r} \cdot f. \quad (31)$$

The mercury should compensate for the resulting frequency shift at a level of 90% or more. The current would therefore generate an artificial EDM signal of magnitude

$$|d| = 0.1 \frac{\mu_n \mu_0 I}{E} \cdot f. \quad (32)$$

As shown above, leakage currents are normally of the order of 1 nA. If the current travels an azimuthal distance of 10 cm around the 47 cm diameter trap, the applied electric field of $E = 1$ MV/m would give a false signal of order 0.1×10^{-27} e cm. Fig. 18 shows the binned weighted-average frequency shifts (i.e., the departures from the fitted Ramsey curves of the individual measurement cycles) as a function of the leakage current. The frequency shifts are multiplied by the product of the polarities of the electric and magnetic fields. No dependence on leakage current is apparent.

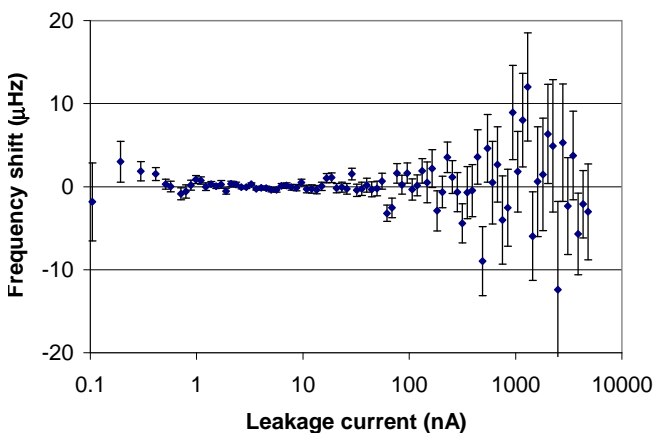


FIG. 18: (Color online) Frequency shifts (multiplied by the polarities of the electric and magnetic fields) as a function of leakage current.

The displacement current as the voltage is ramped up and down was typically $1 \mu\text{A}$. The magnitude of this, along with the known capacitance of the trap, provided the necessary evidence that the applied voltage was

reaching the trap. The current flowing through the trap was not measured directly. The measured current included currents flowing in the high-voltage feedthrough and cable assembly, and it therefore should be regarded as an upper limit for the current that flowed through the trap.

E. HV AC ripple

Changes in precession frequency may be caused by oscillating magnetic fields at non-resonant frequencies through Bloch-Siegert-Ramsey type effects [60]. An example in this class is a “ripple” on the high voltage, which would generate an oscillating displacement current in the storage chamber and thereby an oscillating B field. The ripple amplitude may change with the sign of the high voltage, producing slightly different frequency shifts for each of the two high voltage polarities.

Consider the presence of an oscillating field $\vec{B}_2 \sin \omega_2 t$ in addition to the static field \vec{B}_0 and the resonant alternating field \vec{B}_1 . During the storage time T_s , when \vec{B}_1 is off, the magnetic field in the trap is

$$\vec{B}_t = B_0 \hat{k} + B_2 \sin \omega_2 t \hat{i}. \quad (33)$$

For $B_2 \ll B_0$ and $\omega_2 \gg T_s^{-1}$, the time-averaged magnitude of this field is

$$\langle B_t \rangle \approx B_0 \left(1 + \left(\frac{B_2}{2B_0} \right)^2 \right). \quad (34)$$

The precession frequency therefore becomes

$$\nu'_0 = \nu_0 \left(1 + \left(\frac{B_2}{2B_0} \right)^2 \right), \quad (35)$$

where ν_0 is the frequency in the absence of \vec{B}_2 .

The most probable source of an AC magnetic field is the 20 kHz oscillator that drives the high-voltage stack. This current keeps the capacitors charged against the losses due to the monitoring current. If the driving frequency is ω_2 and the monitoring current is I_s , the voltage associated with this current is

$$\mathcal{E} = \frac{I_s}{\omega_2 C}, \quad (36)$$

where C is the capacitance of the stack. For the fifteen-stage stack with one 3.6 nF capacitor per stage, $\omega_2 = 1.3 \times 10^5$ rad/s and $I_s = 100 \mu\text{A}$, equation (36) yields $\mathcal{E} = 3$ V.

The capacitance of the trap, as calculated for a pair of parallel plates, is 15 pF, which, at 20 kHz, has an impedance of 0.5 M Ω . This shorts out the DC resistance of the trap. Between the stack and the trap is a 1 G Ω resistor chain, so that 3 V produces a 3 nA alternating current. This current flows through the trap as a

displacement current and produces an AC magnetic field whose magnitude, averaged over the volume of the trap, is of the order of 1 fT. This would give a frequency shift of $\approx 10^{-17}$ Hz and a systematic error in the EDM at the level of $\approx 10^{-36}$ e cm, which is a completely negligible effect.

AC fields at mains frequency are another possible cause of concern. There is no differential ripple visible on the HV at the level of a few volts. Sampling is done at 5 Hz with a bandwidth of 20 kHz, so any 50 Hz ripple would show up as beats. This is certainly absent at the level of, say, 50 V, which would give a false EDM of 0.01×10^{-27} e cm.

Low-frequency AC fields were sought by means of a pickup coil in conjunction with a phase-sensitive detector. Shifts in R from this source at the level of 0.02 ppm could not be ruled out. Cancellations in the corresponding EDM signal from reversals of the electric and magnetic fields would reduce any net contribution to below the level of 0.01×10^{-27} e cm.

1. Electric forces

Another possible source of systematic error arises from electrostatic forces, which may move the electrodes slightly. In conjunction with a magnetic field gradient, an HV-dependent shift in the ratio would then appear. This was sought by looking for an EDM-like signal but with a frequency shift proportional to $|\mathbf{E}|$ instead of to \mathbf{E} . The $|\mathbf{E}|$ signal, at $(-2.4 \pm 3.8) \times 10^{-26}$ e cm, was consistent with zero. If the HV magnitudes were slightly different for the two signs of \mathbf{E} , this effect would generate a false EDM signal. Study of the measured HV and of the charging currents show that the HV magnitude was the same for both polarities to within an uncertainty of about 1%. This systematic uncertainty is therefore 1% of the $|\mathbf{E}|$ uncertainty, i.e. 0.4×10^{-27} e cm.

VI. THE DATA-ACQUISITION PROCESS

A data-taking run lasted for up two days and involved a sequence of operations built around the continuous repetition of the basic Ramsey measurement cycle outlined in Section IV. This cycle lasted for approximately four minutes, and involved filling the trap with polarized neutrons and mercury, applying the separated oscillating fields sequence, releasing and counting the neutrons in the original spin state, and finally releasing and counting the neutrons in the other spin state. Each cycle gave rise to a single neutron frequency measurement. Approximately once per hour, the direction of the electric field was reversed. The operation was controlled by a PC running LabVIEW-based software.[84]

A. Filling

The trap was filled for 20 s, corresponding to approximately 1.3 filling time constants, after which the density of UCN was about 2 cm^{-3} . The polarization at this time was approximately 75%. The stored neutrons had their spins aligned antiparallel to the magnetic field in the trap (denominated “spin up”). At this point the neutron door was closed, and the door from the mercury prepolarizing cell was opened for 1 s, allowing the polarized mercury atoms to enter.

B. Ramsey sequence

The Ramsey sequence then began, with a 2 s interval of rotating magnetic field \mathbf{B}'_1 (in the horizontal, or xy , plane) to allow the mercury polarization to precess down into the xy plane, followed by a 2 s interval of (horizontal) oscillating field \vec{B}_1 to turn the neutron polarization in similar fashion. The \mathbf{B}_1 field was aligned with the cylinder axis of the shield and it was generated by a Helmholtz pair of current-carrying wire turns on the vacuum vessel. The current was provided by an HP 3325B frequency synthesiser[85]. The inner magnetic shield acted as a return for the flux. The \mathbf{B}'_1 field (for the mercury) was a superposition of two perpendicular linear oscillating fields, 90° out of phase, generated in an identical manner by their own Helmholtz pairs. The simple nature of the coils, and the distorting effects of eddy currents in the vacuum chamber wall and other metal parts, caused the oscillating field to vary in strength by about 10% over the volume of the neutron trap. Conveniently, the rapid motion of the mercury and neutrons inside the trap provided sufficient averaging in the 2 s duration chosen for each r.f. pulse interval that, in spite of this inhomogeneity, there was a negligible loss of polarization while turning the polarization vectors into the xy plane. The fact that the neutrons remained relatively undisturbed during the four-second period after the closing of the neutron door and before the \mathbf{B}_1 pulse was applied allowed the neutron velocity distribution to relax towards isotropy, and the spatial distribution to relax towards uniformity. This should have minimized any systematic $\mathbf{v} \times \mathbf{E}$ effect arising from the Lorentz transformation of the electric field into the neutrons’ rest frame.

A 130 s interval T_{fp} followed in which the spin polarizations precessed freely in the xy plane about the \mathbf{B}_0 and \mathbf{E} fields. The choice of the length of T_{fp} depended upon several factors: (i) the storage lifetime of neutrons in the trap (about 200 s); (ii) the T_2 relaxation time of the neutrons (about 600 s, although times as long as 1000 s were seen under the best conditions); (iii) the resulting width of the resonance; (iv) the dead time spent in filling and emptying the trap, since the sensitive period T_{fp} should be as long as possible in comparison to them; (v) the signal-to-noise and the depolarization time of the mercury, which affect the accuracy of the frequency mea-

surement; and (vi) the needs of other users of the TGV neutron source, whose measurement cycles had to be interleaved with those of the EDM experiment. The maximum statistical sensitivity was achieved by maximizing, as far as possible, the quantity $\alpha ET_{fp} \sqrt{N_b/T_{tot}}$, where T_{tot} is the total time taken for the measurement cycle and N_b is the number of neutrons per batch cycle. This function is, in fact, rather flat in the region of the 130 s storage time that was used.

C. Counting

The free precession was brought to an end when the frequency synthesiser was gated on to the coil to provide the second 2 s interval of the oscillating B_1 field. Immediately afterwards, the door of the trap was opened. The polarizing foil then served as an analyzer and let through to the detector only those neutrons that project into their original spin-up state. After 8 s of counting, a fast-adiabatic-passage spin-flip coil, adjacent to the polarizer, was energized. The spin-down neutrons, which had until this time been unable to pass the polarizer, then received a 180° spin flip whenever they traversed the spin-flip coil. This permitted them to pass through the polarizer and on to the detector. They were counted in a separate scaler for 20 s, before the system reverted to continued counting of the spin-up neutrons for a final 12 s. Counting the spin-down neutrons served a triple purpose: it increased the sensitivity of the experiment by increasing the number of neutrons counted; it emptied the trap of neutrons that would be in the “unwanted” spin state when refilling at the beginning of the next cycle; and finally, it provided a way of eliminating noise that would be introduced by fluctuations, additional to those of normal counting statistics, in the initial number of stored neutrons after filling. The spin-up and spin-down counts belong to different Ramsey resonance patterns that are 180° out of phase. Splitting the spin-up counting into two periods and inserting the spin-down counting in between them allowed us approximately to equalise the efficiency of detection of the UCN leaving the trap in each state.

The first batch of any run is different from any of the others, as the neutron trap and guides are initially empty; for other batches there is likely to be some remnant population from the previous batch. In consequence the first batch often had an anomalously low total neutron count (and would normally be excluded from analysis).

D. Timing

The timing of the various stages of the measurement cycle was controlled by a dedicated microprocessor. It was installed as a CAMAC unit so that at the start of a run the interval lengths to be used, and the corresponding states of the various valves and relays, could be loaded

into the microprocessor memory from the PC that was in overall control of the data acquisition.

After it had started a cycle, the PC became completely passive with respect to timing. It received signals from the timer that told it the logical state of each hardware control. As each cycle neared its end, the PC awaited an end-of-sequence signal from the timer, at which point it immediately restarted the timer sequence for the next cycle. This ensured that the timing within the cycle, which could potentially influence the number of neutrons counted, could not be affected by the state of the high voltage in some unforeseen way through the action of the software. End-of-cycle tasks such as storing the data on disk and reprogramming the frequency synthesizer were carried out during the first few seconds of the subsequent cycle.

E. High-voltage control

The high voltage was controlled by a separate PC, and the associated controlling and monitoring electronics were kept entirely separate from the data-acquisition electronics. The PCs were networked via a common Ethernet hub. At the start of the run, and after each Ramsey measurement period, the data acquisition PC issued a request to set the appropriate voltage for the upcoming batch. The high-voltage PC transmitted in return a summary of measurements that it had made, such as the average voltage, leakage current, maximum current and so on, during the Ramsey measurement period that has just been completed. These data were stored along with all of the other information relating to that particular measurement cycle. Keeping the high voltage control separate from the data acquisition system minimised the possibility of some unforeseen interaction that might result in a false EDM signal. The initial polarity of the high voltage at the start of the run was chosen randomly by the software.

The high voltage changed with a pattern that repeated every 32-40 measurement cycles (collectively known as a “dwell”), the exact sequence being programmed as desired at the start of the run. There were typically 16 cycles with the electric field applied, say, parallel to the magnetic field, followed by two or four cycles at zero electric field, before the sequence was repeated with the electric field reversed. The electric field did not normally attain its full value until the second cycle of each dwell, because it took a significant amount of time to reverse the polarity and to ramp up the voltage. Only the 40 s period during which the neutrons were being counted was used to change the electric field; the voltage was frozen at the start of the measurement cycle, allowing it to settle and the leakage currents to fall during the neutron filling period so that it was stable during the sensitive Ramsey measurement period. Data taken during the first batch cycle of each high-voltage dwell are therefore valid, and are used in the analysis, but have a reduced sensitivity

relative to the majority of other cycles because of their lower electric fields. In principle, it would have been possible to ramp up fast enough to complete the polarity change within one 40 s period, but doing so would have increased both the displacement current and the probability of sparks occurring.

Thus, the electric field is taken through a cycle of changes that has a repetition period of about 2 hours. The length of this period was chosen with the following considerations in view: The magnetic field had slow drift noise, or what might be called “ $1/f$ ” noise, which, if not treated properly, might have made a significant contribution to the statistical error on the measurement of the EDM. The use of the electric field reversal sequence with a period T_E makes it possible to reduce the noise contributions coming from the spectral components of the drift with period T_{sp} by a factor which is approximately T_{sp}/T_E . Thus, shortening the period for the electric field sequence increased the attenuation for the drift noise at very low frequencies and extended the attenuating effects to higher frequencies. Furthermore, the system was constrained by the behavior of the mercury; it was usually necessary to end a run after a day or two in order to discharge-clean the trap so as to restore the mercury depolarization time. Since it was clearly desirable to have several complete high-voltage dwell periods within each run, one hour was a reasonable maximum time limit between polarity reversals. The disadvantage of shorter dwell sequences is that more time would have been spent at low voltages while the field was being ramped; and, in addition, the mercury depolarization time took an hour or so to recover from the dramatic fall that it suffered at each polarity reversal (see Fig. 14).

Study of the measured HV and of the charging currents show that the HV magnitude was the same for both polarities to within an uncertainty of about 1%.

F. Neutron frequency tracking

The mercury frequency ν_{Hg} for each cycle was used to derive a first-order estimate

$$\nu'_0 = \nu_{Hg} \frac{\gamma_n}{\gamma_{Hg}} \quad (37)$$

for the neutron resonant frequency. This allowed the applied synthesizer frequency ν_1 to be adjusted on a cycle-by-cycle basis in order to track variations in the magnetic field. The frequency ν_1 was made to differ from ν'_0 by an amount

$$\delta\nu = \nu'_0 - \nu_1 \quad (38)$$

where $\Delta\nu$ is the linewidth given by equation (13) and f was chosen sequentially to be -0.55, +0.45, -0.45, +0.55, so as to follow the pairs of working points on either side of the central fringe of the resonance as shown in Fig. 3.

G. Measurement and storage of data

The state of the experiment was monitored and recorded using 24-bit scalars and 12-bit, 10 V ADCs that were read at various points during each measurement cycle, as well as by the 16-bit ADC used to record the oscillating mercury signal. The values of about fifty parameters were written to disk for each cycle. These parameters included the neutron counts for each of the two spin states; neutron counts registered by the flux monitor on the input guide tube; the frequency of the applied oscillating \vec{B}_1 field; the fitted mercury frequency, amplitude and depolarization time, with their associated uncertainties; the high voltage magnitude and polarity; average and maximum leakage currents during the Ramsey measurement period; and various supplemental information, such as the temperature and humidity of the environment. The mercury ADC readings were stored in separate files, in case the need should arise to reanalyze and refit them. For each run, a multichannel analyzer (LeCroy[86] qVt module) recorded the pulse-height spectrum from the neutron detector, and this spectrum was also recorded on disk so that the performance of the detector could be monitored over time. In addition, values for the voltage and current in the HV system were digitised at a rate of 5 Hz, and these readings were also recorded separately so that the high-voltage performance of the system could be examined in detail for any given run.

A single run typically lasted for one to two days, and therefore incorporated about 300 batch cycles.

VII. CONCLUSION

We have presented here a complete description of the apparatus used in the experimental measurement of the electric dipole moment of the neutron at ILL, Grenoble, and discussed many aspects of the hardware that could have introduced systematic errors into the results. The equipment was used to take data from 1996 until 2002, at which time it was decommissioned. At the time of writing, this experiment has provided the world’s most sensitive limit on the neutron EDM.

Acknowledgments

We acknowledge with gratitude the contributions of Prof. N.F. Ramsey, original pioneer of the entire series of neutron EDM experiments, for his invaluable interest and support throughout this long program of work. During the many years of research and development that lie behind this publication, there have been many significant individual contributions. Here, we would like to acknowledge the contributions made by Ph.D. students from the University of Sussex to the previous neutron EDM experiment, upon which the apparatus for this measurement

was strongly based and in whose theses detailed prescriptions for many of the early experimental techniques can be found, namely A.R. Taylor (1977); T. Sumner (1979); S.M. Burnett (1982); P. Franks (1986); P.M.C. de Miranda (1987); N. Crampin (1989); and D.J. Richardson (1989). One of us (DJM) benefitted from an ILL studentship. Much of the detailed on-site work with neutrons at the ILL was carried out by several generations of Research Fellows and engineers, and in this regard we would particularly like to thank R. Golub, J. Morse, H. Prosper and D.T. Thompson. Prof. L. Hunter alerted us to the possibility of a geometric-phase-induced systematic effect caused by the “conspiracy” between $\partial B_z/\partial z$ and the $\mathbf{v} \times \mathbf{E}$ effect. We would like to thank Prof. C. Cohen-Tannoudji for useful discussion relating to fre-

quency shifts caused by the mercury reading light. Prof. A. Serebrov of PNPI assisted us greatly with the provision of high-quality neutron guides. Prof. Lobashev, also of PNPI, helped us to obtain our first quartz-walled neutron containment vessel, and Natasha Ivanov helped us to obtain various optical components. The experiments would not have been possible at all without the cooperation and provision of neutron facilities by the ILL itself. This work has been funded by the U.K. Science and Technology Facilities Council (STFC) and by its predecessor, the Particle Physics and Astronomy Research Council (PPARC). Much of the early magnetometry work, in particular that carried out at the University of Washington, was supported by NSF grant PHY-8711762.

-
- [1] C. Baker et al., Phys. Rev. Lett. **97**, 131801 (2006).
 [2] N. Ramsey, Rep. Prog. Phys. **45**, 95 (1982).
 [3] S. Barr and W. Marciano, in *CP Violation*, edited by C. Jarlskog (World Scientific, Singapore, 1989).
 [4] R. Sachs, *The Physics of Time Reversal* (University of Chicago Press, 1987).
 [5] C. Wu et al., Phys. Rev. **105**, 1413 (1957).
 [6] A. Angelopoulos et al., Phys. Lett. B **44**, 43 (1998).
 [7] A. Alavi-Harati et al., Phys. Rev. Lett. **84**, 408 (2000).
 [8] J. Adams et al., Phys. Rev. Lett. **80**, 4123 (1998).
 [9] G. Lüders, Kgl. Danske Videnskab. Selskab, Mat.-fys. Medd. **28** (1954).
 [10] J. Schwinger, Phys. Rev. **91**, 720 (1953).
 [11] J. Schwinger, Phys. Rev. **94**, 1366 (1953).
 [12] J. Christenson, J. Cronin, V. Fitch, and R. Turlay, Phys. Rev. Lett. **13**, 138 (1964).
 [13] B. Aubert et al., Phys. Rev. Lett. **87**, 091802 (2001).
 [14] K. Abe et al., Phys. Rev. Lett. **87**, 091802 (2001).
 [15] D. Kirkby and Y. Nir, Phys. Lett. B **592**, 136 (2004).
 [16] A. Alavi-Harati et al., Phys. Rev. Lett. **83**, 22 (1999).
 [17] S. Barr, Int. J. Mod. Phys. A **8**, 209 (1993).
 [18] C. Jarlskog, ed., *CP Violation* (World Scientific, Singapore, 1989).
 [19] J. Ellis, Nucl. Instr. Meth. A **284**, 33 (1989).
 [20] X.-G. He, B. McKellar, and S. Pakvasa, Int. J. Mod. Phys. A **4**, 5011 (1989).
 [21] J. Smith, E. Purcell, and N. Ramsey, Phys. Rev. **108**, 120 (1957).
 [22] P. Miller, W. Dress, J. Baird, and N. Ramsey, Phys. Rev. Lett. **19**, 381 (1967).
 [23] C. Shull and R. Nathans, Phys. Rev. Lett. **19**, 384 (1967).
 [24] W. Dress, J. Baird, P. Miller, and N. Ramsey, Phys. Rev. **170**, 1200 (1968).
 [25] V. Cohen, R. Nathans, H. Silsbee, et al., Phys. Rev. **177**, 1942 (1969).
 [26] J. Baird, P. Miller, W. Dress, and N. Ramsey, Phys. Rev. **179**, 1285 (1969).
 [27] S. Apostolescu, D. Ionescu, M. Ionescu-Bujor, et al., Rev. Roumaine Phys. **15**, 3 (1970).
 [28] W. Dress, P. Miller, and N. Ramsey, Phys. Rev. D **7**, 3147 (1973).
 [29] W. Dress, P. Miller, J. Pendlebury, et al., Phys. Rev. D **15**, 9 (1977).
 [30] I. Altarev, Y. Borisov, A. Brandin, et al., Nucl. Phys. A **341**, 269 (1980).
 [31] I. Altarev, Y. Borisov, N. Borovikova, et al., Phys. Lett. B **102**, 13 (1981).
 [32] J. Pendlebury, K. Smith, R. Golub, et al., Phys. Lett. B **136**, 327 (1984).
 [33] I. Altarev, Y. Borisov, N. Borovikova, et al., JETP Lett. **44**, 460 (1986).
 [34] K. Smith, N. Crampin, J. Pendlebury, et al., Phys. Lett. B **234**, 191 (1990).
 [35] I. Altarev, Y. Borisov, N. Borikova, et al., Phys. Lett. B **276**, 242 (1992).
 [36] I. Altarev, Y. Borisov, N. Borikova, et al., Phys. Atomic Nuclei **59**, 1152 (1996).
 [37] P. Harris, C. Baker, K. Green, et al., Phys. Rev. Lett. **82**, 904 (1999).
 [38] M. Romalis, W. Griffith, and E. Fortson, Phys. Rev. Lett. **86**, 2505 (2001).
 [39] B. Regan, E. Commins, C. Smidt, and D. DeMille, Phys. Rev. Lett. **88**, 071805 (2002).
 [40] J. Hudson, B. Sauer, M. Tarbutt, and E. Hinds, Phys. Rev. Lett. **89**, 272701 (2002).
 [41] M. Kozlov and D. DeMille, Phys. Rev. Lett. **89**, 133001 (2002).
 [42] O. Lebedev, K. Olive, M. Pospelov, and A. Ritz, Phys. Rev. D **70**, 016003 (2004).
 [43] S. Abel and O. Lebedev, JHEP **0601**, 133 (2006).
 [44] N. Ramsey, in *Proc. XIV Int. Conf. Atomic Physics* (AIP, New York, 1994), p. 3.
 [45] I. Khriplovich and S. Lamoreaux, *CP Violation without Strangeness* (Springer, 1996).
 [46] F. Shapiro, Sov. Phys. Usp. **11**, 345 (1968).
 [47] R. Golub and J. Pendlebury, Contemp. Phys. **13**, 519 (1972).
 [48] S. Lamoreaux and R. Golub, Phys. Rev. Lett. **98**, 149101 (2007).
 [49] J. Pendlebury et al., Phys. Rev. A **70**, 032102 (2004).
 [50] R. Golub and J. Pendlebury, Rep. Prog. Phys. **42**, 439 (1979).
 [51] Y. Zel'dovich, Sov. Phys. JETP **9**, 1389 (1959).
 [52] A. Stoika, A. Strelkov, and M. Hetzelt, Z. Phys. B **29**, 349 (1978).
 [53] W. Lanford and R. Golub, Phys. Rev. Lett. **39**, 1509

- (1977).
- [54] Montedison Group, Montefluos, Foro Buonaparte 31, Milano, Italy.
- [55] J. Bates, Phys. Lett. A **88**, 427 (1982).
- [56] H. Goldenberg, D. Kleppner, and N. Ramsey, Phys. Rev. **123**, 530 (1961).
- [57] N. Ramsey, *Molecular Beams* (Oxford University Press, 1956).
- [58] N. Ramsey, Rev. Mod. Phys. **62**, 541 (1990).
- [59] D. May, Ph.D. thesis, University of Sussex (1999).
- [60] N. Ramsey, Phys. Rev. **100**, 1191 (1955).
- [61] F. Bloch and A. Siegert, Phys. Rev. **57**, 522 (1940).
- [62] C. Baker et al., Phys. Rev. Lett. **98**, 149102 (2007).
- [63] A. Steyerl, H. Nagel, F.-X. Schreiber, et al., Phys. Lett. A **116**, 347 (1986).
- [64] A. Steyerl and S. S. Malik, Nucl. Instr. Meth. A **284**, 200 (1989).
- [65] A. Taylor, Ph.D. thesis, University of Sussex (1977).
- [66] S. Al-Ayoubi, Ph.D. thesis, University of Sussex (2002).
- [67] W. Mampe and J. P. Bugeat, Phys. Lett. A **78**, 293 (1980).
- [68] R. Herdin, A. Steyerl, A. Taylor, et al., Nucl. Instr. Meth. **148**, 353 (1977).
- [69] P. de Miranda, Ph.D. thesis, University of Sussex (1987).
- [70] L. Alston, *High Voltage Technology* (Oxford University Press, 1968).
- [71] M. van der Grinten, J. Pendlebury, D. Shiers, et al., Nucl. Instr. Meth. A **423**, 421 (1999).
- [72] K. Green, P. Harris, P. Iaydjiev, et al., Nucl. Instr. Meth. A **404**, 381 (1998).
- [73] H. Dehmelt, Phys. Rev. **105**, 1487 (1957).
- [74] H. Dehmelt, Phys. Rev. **105**, 105 (1957).
- [75] Y. Chibane, J. Pendlebury, and K. Smith, Meas. Sci. Technol. **6**, 11671 (1995).
- [76] C. Cohen-Tannoudji and J. Dupont-Roc, Phys. Rev. A **5**, 968 (1972).
- [77] A. Corney, *Atomic and Laser Spectroscopy* (Oxford University Press, 1968).
- [78] Magnetic Shields Ltd., Headcorn Rd., Staplehurst, Kent TN12 0DS, U.K.
- [79] T. Sumner, J. Pendlebury, and K. Smith, J. Phys. D **20**, 1095 (1987).
- [80] N. Ramsey, Acta Phys. Hung. **55**, 117 (1984).
- [81] D. Keppner, H. Goldenberg, and N. Ramsey, Phys. Rev. **126**, 603 (1962).
- [82] Bartington Instruments Ltd., 10 Thorney Leys Business Park, Witney, Oxford, OX28 4GG England. <http://www.bartington.com/form.htm>.
- [83] Bonar Wallis Electronics Ltd., Worthing, U.K.
- [84] National Instruments corporation, 6504 Bridge Point Parkway, Austin, TX 78730-5039, U.S.A.
- [85] Hewlett-Packard inc., Palo Alto, CA, U.S.A.
- [86] LeCroy Research Systems, 700 Chestnut Ridge Road, Chestnut Ridge, NY 10977, U.S.A.